






















In situ investigation of an organic micro-globule and its mineralogical context within a Ryugu “sand” grain

Van T. H. PHAN ^{1*}, Pierre BECK¹, Rolando REBOIS¹, Eric QUIRICO¹, Takaaki NOGUCHI ², Toru MATSUMOTO^{2,3}, Akira MIYAKE², Yohei IGAMI², Mitsutaka HARUTA⁴, Hikaru SAITO^{5,6}, Satoshi HATA^{7,8}, Yusuke SETO⁹, Masaaki MIYAHARA ¹⁰, Naotaka TOMIOKA ¹¹, Hope A. ISHII ¹², John P. BRADLEY¹², Kenta K. OHTAKI¹², Elena DOBRICÁ ¹², Hugues LEROUX ¹³, Corentin LE GUILLOU¹³, Damien JACOB¹³, Francisco de la PEÑA¹³, Sylvain LAFORET¹³, Maya MARINOVA¹⁴, Falko LANGENHORST¹⁵, Dennis HARRIES ¹⁶, Neyda M. ABREU¹⁷, Jennifer GRAY¹⁸, Thomas ZEGA ¹⁹, Pierre-M. ZANETTA¹⁹, Michelle S. THOMPSON²⁰, Rhonda STROUD²¹, Jérémie MATHURIN ²², Alexandre DAZZI²², Emmanuel DARTOIS²³, Cécile ENGRAND ²⁴, Kate BURGESS ²⁵, Brittany A. CYMES ²⁶, John C. BRIDGES²⁷, Leon HICKS^{27,28}, Martin R. LEE ²⁹, Luke DALY ^{29,30,31}, Phil A. BLAND³², Michael E. ZOLENSKY ³³, David R. FRANK¹², James MARTINEZ³⁴, Akira TSUCHIYAMA^{35,36,37}, Masahiro YASUTAKE³⁸, Junya MATSUNO³⁵, Shota OKUMURA², Itaru MITSUKAWA², Kentaro UESUGI³⁸, Masayuki UESUGI ³⁸, Akihisa TAKEUCHI³⁸, Mingqi SUN^{36,37,39}, Satomi ENJU⁴⁰, Aki TAKIGAWA⁴¹, Tatsuhiro MICHIKAMI⁴², Tomoki NAKAMURA⁴³, Megumi MATSUMOTO⁴³, Yusuke NAKAUCHI⁴⁴, Masanao ABE^{44,45}, Satoru NAKAZAWA⁴⁴, Tatsuaki OKADA^{44,45}, Takanao SAIKI⁴⁴, Satoshi TANAKA^{44,45}, Fuyuto TERUI⁴⁶, Makoto YOSHIKAWA^{44,45}, Akiko MIYAZAKI⁴⁴, Aiko NAKATO⁴⁴, Masahiro NISHIMURA⁴⁴, Tomohiro USUI⁴⁴, Toru YADA⁴⁴, Hisayoshi YURIMOTO ⁴⁴, Kazuhide NAGASHIMA ¹², Noriyuki KAWASAKI ⁴⁷, Naoya SAKAMOTOA⁴⁸, Peter HOPPE⁴⁹, Ryuji OKAZAKI⁵⁰, Hikaru YABUTA¹⁰, Hiroshi NARAOKA⁵⁰, Kanako SAKAMOTO⁴⁴, Shogo TACHIBANA ⁵¹, Sei-ichiro WATANABE⁵², and Yuichi TSUDA⁴⁴

¹Institut de Planétologie et d'Astrophysique de Grenoble (IPAG), CNRS, Université Grenoble Alpes, Grenoble, France

²Division of Earth and Planetary Sciences, Kyoto University, Kyoto, Japan

³The Hakubi Center for Advanced Research, Kyoto University, Kyoto, Japan

⁴Institute for Chemical Research, Kyoto University, Kyoto, Japan

⁵Institute for Materials Chemistry and Engineering, Kyushu University, Fukuoka, Japan

⁶Pan-Omics Data-Driven Research Innovation Center, Kyushu University, Fukuoka, Japan

⁷Interdisciplinary Graduate School of Engineering Sciences, Kyushu University, Fukuoka, Japan

⁸The Ultramicroscopy Research Center, Kyushu University, Fukuoka, Japan

⁹Department of Geosciences, Osaka Metropolitan University, Osaka, Japan

¹⁰Department of Earth and Planetary Systems Science, Hiroshima University, Hiroshima, Japan

¹¹Kochi Institute for Core Sample Research, X-Star, JAMSTEC, Nankoku, Japan

¹²Hawai'i Institute of Geophysics and Planetology, The University of Hawai'i at Mānoa, Honolulu, Hawaii, USA

¹³CNRS, INRAE, Centrale Lille, UMR 8207-UMET-Unité Matériaux et Transformations, Université de Lille, Lille, France

¹⁴CNRS, INRAE, Centrale Lille, Université Artois, FR 2638-IMEC-Institut Michel-Eugène Chevreul, Université de Lille, Lille, France

¹⁵Institut für Geowissenschaften, Friedrich-Schiller-Universität Jena, Jena, Germany

¹⁶European Space Resources Innovation Centre, Luxembourg Institute of Science and Technology, Belvaux, Luxembourg

¹⁷NASA Langley Research Center, Hampton, Virginia, USA

¹⁸Materials Characterization Lab, The Pennsylvania State University Materials Research Institute, University Park, Pennsylvania, USA

¹⁹Lunar and Planetary Laboratory, Department of Planetary Sciences, The University of Arizona, Tucson, Arizona, USA

²⁰Department of Earth, Atmospheric and Planetary Sciences, Purdue University, West Lafayette, Indiana, USA

²¹Buseck Center for Meteorite Studies, Arizona State University, Tempe, Arizona, USA

²²Institut Chimie Physique, CNRS, Univ. Paris-Saclay, Orsay, France

- ²³Institut des Sciences Moléculaires d'Orsay, CNRS, Univ. Paris-Saclay, Orsay, France
²⁴IJCLab, UMR 9012, CNRS, Univ. Paris-Saclay, Orsay, France
²⁵Materials Science and Technology Division, U.S. Naval Research Laboratory, Washington, DC, USA
²⁶U.S. Naval Research Laboratory, Washington, DC, USA
²⁷Space Park Leicester, The University of Leicester, Leicester, UK
²⁸School of Geology, Geography and the Environment, The University of Leicester, Leicester, UK
²⁹School of Geographical and Earth Sciences, The University of Glasgow, Glasgow, UK
³⁰Australian Centre for Microscopy and Microanalysis, The University of Sydney, Sydney, New South Wales, Australia
³¹Department of Materials, The University of Oxford, Oxford, UK
³²School of Earth and Planetary Sciences, Curtin University, Perth, Western Australia, Australia
³³ARES, NASA Johnson Space Center, Houston, Texas, USA
³⁴Jacobs Engineering, Dallas, Texas, USA
³⁵Research Organization of Science and Technology, Ritsumeikan University, Kusatsu, Japan
³⁶CAS Key Laboratory of Mineralogy and Metallogeny, Guangdong Provincial Key Laboratory of Mineral Physics and Materials, Guangzhou Institute of Geochemistry, Chinese Academy of Sciences (CAS), Guangzhou, China
³⁷CAS Center for Excellence in Deep Earth Science, Guangzhou, China
³⁸Japan Synchrotron Radiation Research Institute, Sayo-gun, Japan
³⁹University of Chinese Academy of Sciences, Beijing, China
⁴⁰Department of Mathematics, Physics, and Earth Science, Ehime University, Matsuyama, Japan
⁴¹Department of Earth and Planetary Science, The University of Tokyo, Tokyo, Japan
⁴²Faculty of Engineering, Kindai University, Hiroshima, Japan
⁴³Department of Earth Science, Tohoku University, Sendai, Japan
⁴⁴Institute of Space and Astronautical Science, Japan Aerospace Exploration Agency, Sagami-hara, Japan
⁴⁵The Graduate University for Advanced Studies, SOKENDAI, Hayama, Japan
⁴⁶Department of Mechanical Engineering, Kanagawa Institute of Technology, Atsugi, Japan
⁴⁷Department of Earth and Planetary Sciences, Hokkaido University, Sapporo, Japan
⁴⁸Creative Research Institution Sousei, Hokkaido University, Sapporo, Japan
⁴⁹Nano- und Mikropartikelforschung, Max Planck Institut für Chemie, Mainz, Germany
⁵⁰Department of Earth and Planetary Sciences, Kyushu University, Fukuoka, Japan
⁵¹UTokyo Organization for Planetary and Space Science, The University of Tokyo, Tokyo, Japan
⁵²Department of Earth and Environmental Sciences, Nagoya University, Nagoya, Japan

***Correspondence**

Van T. H. Phan, Institut de Planétologie et d'Astrophysique de Grenoble (IPAG), Université Grenoble Alpes/CNRS-INSU, UMR 5274, Grenoble F-38041, France.

Email: thi-hai-van.phan@univ-grenoble-alpes.fr

(Received 07 April 2023; revision accepted 14 December 2023)

Abstract—The Hayabusa2 mission from the Japan Aerospace Exploration Agency (JAXA) returned to the Earth samples of carbonaceous asteroid (162173) Ryugu. This mission offers a unique opportunity to investigate in the laboratory samples from a C-type asteroid, without physical or chemical alteration by the terrestrial atmosphere. Here, we report on an investigation of the mineralogy and the organo-chemistry of Hayabusa2 samples using a combination of micro- and nano-infrared spectroscopy. Particles investigated with conventional FTIR spectroscopy have spectra dominated by phyllosilicate-related absorption, as observed for samples of CI-chondrites, selected ungrouped carbonaceous chondrites, and selected hydrated micrometeorites. Ryugu samples show smaller sulfate-related absorption than CI-chondrites. Our samples that were only briefly exposed to the Earth atmosphere show absorptions related to molecular water, revealing fast terrestrial contamination of the spectral signature at 3 μm . Overall, our FTIR data are in agreement with other work done on Ryugu samples, revealing a low degree of mineralogical variability across Ryugu samples. AFM-IR mapping of the grains shows the presence of a micrometer-sized organic globule in one of our analyzed grains. The AFM-IR spectra obtained on this globule are similar to IR spectra obtained on IOM suggesting that it is constituted of refractory organic matter. This globule may host silicate in its interior, with a different mineralogy than bulk Ryugu phyllosilicate. The shape, presence of peculiar silicate, and the nature of organic constituting the globule

point toward a pre-accretionary origin of this globule and that at least part of Ryugu organics were inherited from the protosolar nebulae or the interstellar media. Altogether, our results show the similarities between Ryugu samples and CI chondrites.

INTRODUCTION

In late 2020, samples of the dark asteroid Ryugu (Cb spectral type) were returned to the Earth after a >5 billions of kilometers trip made by the Hayabusa2 spacecraft, built by the Japan Aerospace Exploration Agency (JAXA). Early investigations of the samples revealed that Ryugu particles share many characteristics of chemically primitive but also highly aqueously altered CI group of carbonaceous chondrites (Nakamura et al., 2022; Noguchi et al., 2022; Yada et al., 2021; Yokoyama et al., 2022). Therefore, the Hayabusa2 samples offer the unique opportunity to investigate exceptionally fresh CI material. Hayabusa2 samples were protected from interaction with the oxidizing terrestrial atmosphere from capsule recovery to curation process, and they were also protected from thermal and mechanical modification during atmospheric entry.

The relation to CI meteorites was drawn from chemical, mineralogical, and isotopic similarities (Dartois et al., 2023; Nakamura et al., 2022; Naraoka et al., 2023; Noguchi et al., 2022; Yabuta et al., 2023; Yada et al., 2021; Yokoyama et al., 2022). CI chondrites show an interplay of ingredients down to the submicrometer scale (Le Guillou et al., 2014; Tomeoka & Buseck, 1988), which requires analytical techniques with submicrometer spatial resolution to separate their composition and understand their petrographic relations. Infrared spectroscopy (IR) is an effective method and a nondestructive technique for molecular atomic scale vibrations of organic and inorganic compounds in extraterrestrial materials (Beck et al., 2014; Kebukawa et al., 2011; Orthous-Daunay et al., 2013; Phan et al., 2021). However, conventional IR spectrometers use mirror-based optics to focus the beam on the sample, and thus, the spatial resolution is limited by diffraction. This IR diffraction limitation can be overcome by using AFM-IR (atomic force microscopy-infrared spectroscopy), based on the combination of infrared spectroscopy and atomic force microscopy to efficiently distinguish spectral signatures of the different constituents (Dazzi & Prater, 2017; Mathurin et al., 2019). This technique has been successfully applied to extraterrestrial materials (Dartois et al., 2023; Kebukawa et al., 2018; Mathurin et al., 2019; Mathurin, Deniset-Besseau, et al., 2022; Noguchi et al., 2022; Phan et al., 2022; Yabuta et al., 2023; Yesiltas et al., 2021).

Here, we report our work to understand the mineralogy and petrography of fine-grained Ryugu

samples as part of the preliminary examination team (Noguchi et al., 2023) using photothermal AFM-IR spectroscopy. Across our investigations, we gained insights into the mineralogy and chemistry of phyllosilicates, and we report on the discovery of a “large” organic-dominated globule.

MATERIALS AND METHODS

Fine-Grained Ryugu C0105 Samples

After their arrival on Earth in December 2020, the Ryugu samples were transported from JAXA's Extraterrestrial Sample Curation Center in Sagami-hara, Japan, then to the Mineralogy and Petrography fine-grain initial analysis team (Sand team) (Noguchi et al., 2023). Two grains of Ryugu from chamber C (C0105-003200401 and C0105-00380010), designated C0105-0032 and -0038 in the following text, were then sent to University Grenoble Alpes for Micro-FTIR, AFM-IR, and SEM-EDS analyses.

Ryugu fragments were tightly pressed between two diamond windows (type IIa diamond, 3 mm diameter and 500 μm thick), generating to thin and flat samples (1–5 μm thick, with a typical area of 50 \times 50 μm). One of the two windows was removed to avoid interference and to minimize beam intensity loss during transmission mode measurements. This sample preparation significantly reduced scattering artifacts and was well suited for conventional micro-FTIR. These pressed samples were also used for AFM-IR measurements. Typically, meteorite grains were prepared by crushing 10–20 μm fragments between two diamond windows, while the Ryugu samples were collected at around 1–5 μm . Before AFM-IR analysis, all samples were analyzed using conventional micro-FTIR analysis, in order to select regions of interests (ROI).

Methods

Micro-FTIR Spectroscopy

The micro-infrared spectra were measured with a Bruker Hyperion 3000 infrared microscope at the Institut de Planétologie et d'Astrophysique de Grenoble (IPAG, Grenoble, France). Spectra were measured in transmission and obtained by putting the diamond window in a custom-made environmental chamber, which exposes the sample to secondary vacuum, and elevated temperature if needed

(up to 300°C). This procedure enables the removal of molecular water that can perturb the IR spectra in the 3 μm range (4000–3000 cm^{-1}) and also around 1630 cm^{-1} . Spectra were obtained for areas that are typically 50 \times 50 μm .

Atomic Force Microscope-Based Infrared Spectroscopy (AFM-IR) Measurements

AFM-IR analyses were performed on Ryugu samples after the micro-FTIR measurements. IR images and absorption spectra were acquired using a nanoIR3sTM (Bruker) located at IPAG. This system includes an atomic force microscope (AFM) probe, which can scan the sample to generate its topographical image as well as measuring IR absorption by detecting photothermal expansion (Dazzi & Prater, 2017). Detailed descriptions of the NanoIR3sTM (Bruker) were provided in previous publications (e.g., Phan et al., 2022, 2023) together with the measurement of reference materials. Briefly, the excitation laser source is a Carmina laser (from APE company) that covers a part of the mid-IR range, from 2000 to 700 cm^{-1} with its OPO/DFG (optical parametric oscillator and a difference frequency generation) architecture (APE GmbH, Germany), and infrared light in the 2700–4000 cm^{-1} wave number range is supplied by an optical parametric oscillator, Firefly (FF) IR laser (M squared lasers limited, Glasgow, UK). Both contact mode (CM) and tapping IR mode (TM) were used for spectroscopy and imaging measurements. The reference signal (incoming laser intensity) is recorded prior to image and/or spectra collection, and laser alignment optimization is performed before signal acquisition at different wavelengths (or wave numbers) in the scanned range.

AFM-IR images were obtained using the APE laser in TM with a laser power of 8.81%–25% of its maximum and a pulse rate at 340–380 kHz. These analytical conditions were optimized by choosing the lowest laser power that would provide good quality spectra without affecting the sample integrity. It is well known that laser irradiation can alter the structure of macromolecular organics (in particular using highly focused beam like in Raman spectroscopy) and the analytical protocol we used has been constructed and validated in our earlier work on meteorites and coals (Phan et al., 2022, 2023). The images were collected in the range of 2000–700 cm^{-1} at infrared wave numbers of 1720, 1600, 1450, and 1000 cm^{-1} , which correspond to the carbonyl (C O) stretching, sp^2 aromatic (C C), methylene (CH_2) bending and/or carbonate and/or NH_4^+ bending mode, and silicate (Si-O) stretching, respectively. Images were taken through each region of interest (ROI) from each section. In addition, AFM-IR images in the range of 3800–2700 cm^{-1} were acquired using the Firefly laser in CM, which can be resolved into

discrete bands including the stretching of OH (3600–3700 cm^{-1}), asymmetric stretching of CH_3 (2960 cm^{-1}), asymmetric stretching of CH_2 (2930 cm^{-1}), symmetric stretching of CH_3 (2880 cm^{-1}), and symmetric stretching of CH_2 (2860 cm^{-1}) (Beck et al., 2010; Dazzi & Prater, 2017; Jubb et al., 2019; Phan et al., 2022). To better visualize the spatial distribution of different components, composite RGB color images were created by superimposing three different absorption images using the Anasys software. Before overlaying the images, each individual image was realigned to compensate for any small drifts between AFM-IR image recordings. The scan speed of all maps was 0.1 Hz and the scan sizes were from 300 \times 300 to 500 \times 500 points depending the size of ROI.

Local AFM-IR spectra were also obtained for two grains, C0105-0032 and C105-0038 pressed grains. For C0105-0032, the spectra were acquired in TM using the APE laser, while for C0105-0038, the spectra were acquired in CM using both the APE in the range 2000–700 cm^{-1} and the Firefly laser in the range 3800–2700 cm^{-1} . To avoid damaging the samples and obtain high-quality spectra, the incident laser power was kept to 1.22%–5.03% of its maximum and the pulse rate was maintained at 240–300 kHz (Phan et al., 2022, 2023). The IR spectra were optimized at a constant laser power level for each wave number, with the laser power recorded with an IR-sensitive photodetector. Each AFM-IR spectrum was obtained at selected points with a wave number spacing of 4 cm^{-1} and we have used co-averages of three spectra and five spectra for the APE and Firefly laser, respectively. For the spectral range of 2000–700 cm^{-1} , a gold-coated semi-tap probe (PR-EX-TnIR-A-10, 75 \pm 15 kHz, 1–7 N m^{-1}) was used to avoid artifact effects due to the silicon IR absorption and allow to work both CM and TM. For the spectral range of 4000–2700 cm^{-1} , the images and spectra are acquired in CM with “pure contact” model PR-EX-nIR2-1, a resonant frequency of 13 \pm 4 kHz and a spring constant of 0.07–0.4 N m^{-1} .

Scanning Electron Microscopy (SEM) and Energy-Dispersive Spectroscopy (EDS) Measurement

After AFM-IR analysis, the samples were coated with a thin gold (Au) film for observation with a scanning electron microscope in secondary and backscattered electron modes. A JEOL JSM-7000F scanning electron microscope (SEM) equipped with an energy-dispersive spectroscopy (EDS) (JEOL, USA, Inc, Peabody, MA) was used at the Consortium des Moyens Technologiques Communs (CMTC, University Grenoble Alpes, France). EDS maps of carbon (C), oxygen (O), silicate (Si), aluminum (Al), iron (Fe), nickel (Ni), and sulfur (S) were collected at the acceleration voltage of 10 kV and the

beam current of 30 nA. EDS spectra were also collected to drive more details on the global composition of each section ([Supporting Information](#)).

RESULTS

Grain C0105-0032

Using the tapping IR mode (TM), we studied the spatial distribution of organic and mineral infrared signatures throughout the entire surface of the C0105-0032 and C0105-0038. A $5 \times 5 \mu\text{m}$ ROI of C0105-0032 was analyzed with a higher spatial resolution of 500×500 points (e.g., spatial resolution imaging of ~ 10 nm) (Figure 1a). AFM-IR images obtained at different wavelengths show the distribution of different vibrational bonds: carbonyl (C O) (in red, at 1720 cm^{-1}), aromatic (C C) (in pink, at 1600 cm^{-1}), carbonate (CO_3) or CH_2 bending mode groups (in blue at 1450 cm^{-1}), sulfate (SO_4) (in yellow, at 1100 cm^{-1}), and phyllosilicate (Si-O) (in green, at 1000 cm^{-1}) (Figure 1b–f). Figure 2b,c shows a color composite RGB map (1720, 1600, and 1450 cm^{-1} IR intensity) and individual absorption map at 1450, 1100, and 1000 cm^{-1} , together with the locations where full spectra were collected in the $2000\text{--}700 \text{ cm}^{-1}$ range.

These maps enable to identify different domains (Figures 1 and 2). Overall, the most widespread absorption is the band at around 1000 cm^{-1} , which can be attributed to Si-O stretching in phyllosilicates (green area in Figure 2b,c). This observation agrees with the fact that Ryugu fine-grained samples mineralogy is dominated by phyllosilicates (Noguchi et al., [this volume](#)). Isolated blue and violet (Figure 2b,c) areas are also observed in the RGB maps and are interpreted to be micro to sub- μm -sized carbonate grains.

Only a few areas are red in Figure 2a can be explained by pure organics. The map obtained at 1720 cm^{-1} , intended to probe the C O mode, shows a strong correlation to carbonates signatures. Several areas appear yellow in Figure 2c, meaning that they display particularly strong signatures around 1100 cm^{-1} , which may be interpreted by the presence of sulfate.

In order to gain further insights into the constituents of our Ryugu grains, we collected an array of more than 100 single-point AFM-IR spectra in the $2000\text{--}700 \text{ cm}^{-1}$ range (in tapping IR mode), that can be compared to μ -FTIR spectra of the grains as well as to reference spectra of possible mineral components (e.g., saponite, dolomite, calcite) and the Orgueil CI chondrite (Phan et al., 2022) (Figure 2d). We averaged 90 spectra, exhibiting a similar signature (P spectra in Figure 2d) and compared them to 13 different spectra obtained at locations marked P1–P10 and C1–C3. The average spectra (P) in the green region have a strong and narrow absorption at 1000 cm^{-1} , similar

to FTIR spectra observations, which are attributed to phyllosilicate (Si-O), and the best spectral analog to date is a saponite spectrum (Beck et al., 2014), with a possible contribution from serpentine (Dartois et al., 2023).

The C2 and C3 spectra also display strong absorption at 1440 and 880 cm^{-1} band attributed to carbonate (Figure 2d). Carbonates were found in mm-sized grains (Nakamura et al., 2022) and smaller isolated or aggregated grains (Dartois et al., 2023; Yabuta et al., 2023) of a few to $\sim 30 \mu\text{m}$ size. Dolomite is the dominant carbonate in the Ryugu coarse samples (1–8 mm) which were formed by aqueous alteration reactions at low temperature, high pH, and water/rock ratios < 1 (Nakamura et al., 2022). Porous dolomite and magnetite that occur in some frothy layer are thought to have been modified by space weathering processes (Noguchi et al., 2023).

Interestingly, spectrum C1 in the redder location in Figure 2b reveals faint but distinct peaks at 1720 and 1600 cm^{-1} attributed to C O and C C present together with the strong peak at 1000 cm^{-1} implying the presence of organic matter associated with Mg-rich phyllosilicate (Figure 2d). A diffuse organic component within the phyllosilicate matrix may be present in the grain, but in tapping IR mode, these faint organic signatures are generally absent from the AFM-IR spectra (Figure 2d,e) (Phan et al., 2022, 2023). In addition, spectra obtained at the P1–P10 that have different absorption at 1100 and 860 cm^{-1} , probably due to different types of sulfate and/or silicate (Madejová et al., 2017) (Figure 2e).

Grain C0105-0038

The grain of C0105-0038 (Figure 3a) was fractured into several smaller grains, then crushed between two diamond windows (Figure 3b), and the micro-FTIR spectra measured are displayed in Figure 3c. The Ryugu bulk samples infrared transmission we obtained appear similar to those measured for CI chondrites such as Orgueil or Ivuna (Nakamura et al., 2022; Yokoyama et al., 2022). A band at 3690 cm^{-1} is observed, corresponding to an -OH stretching mode in an Mg-rich phyllosilicate. This band is weak in Figure 3c since the pressed sample was particularly thin. In the $3000\text{--}2800 \text{ cm}^{-1}$ range, several bands are observed with peaks at 2952, 2925, 2873, and 2857 cm^{-1} . These peaks are attributed to the asymmetric and symmetric stretching modes of the CH_3 , CH_2 , and CH groups, related to complex interactions between overtones and fundamental vibrations. Spectra obtained in all sections reveal the presence of a sharp feature at 1000 cm^{-1} that can be attributed to phyllosilicate. Unlike the other samples, grain 4 (G4) presents a strong signature at 1440 and 880 cm^{-1} that can be attributed to carbonate bending and in-plane mode, respectively (Phan et al., 2022).

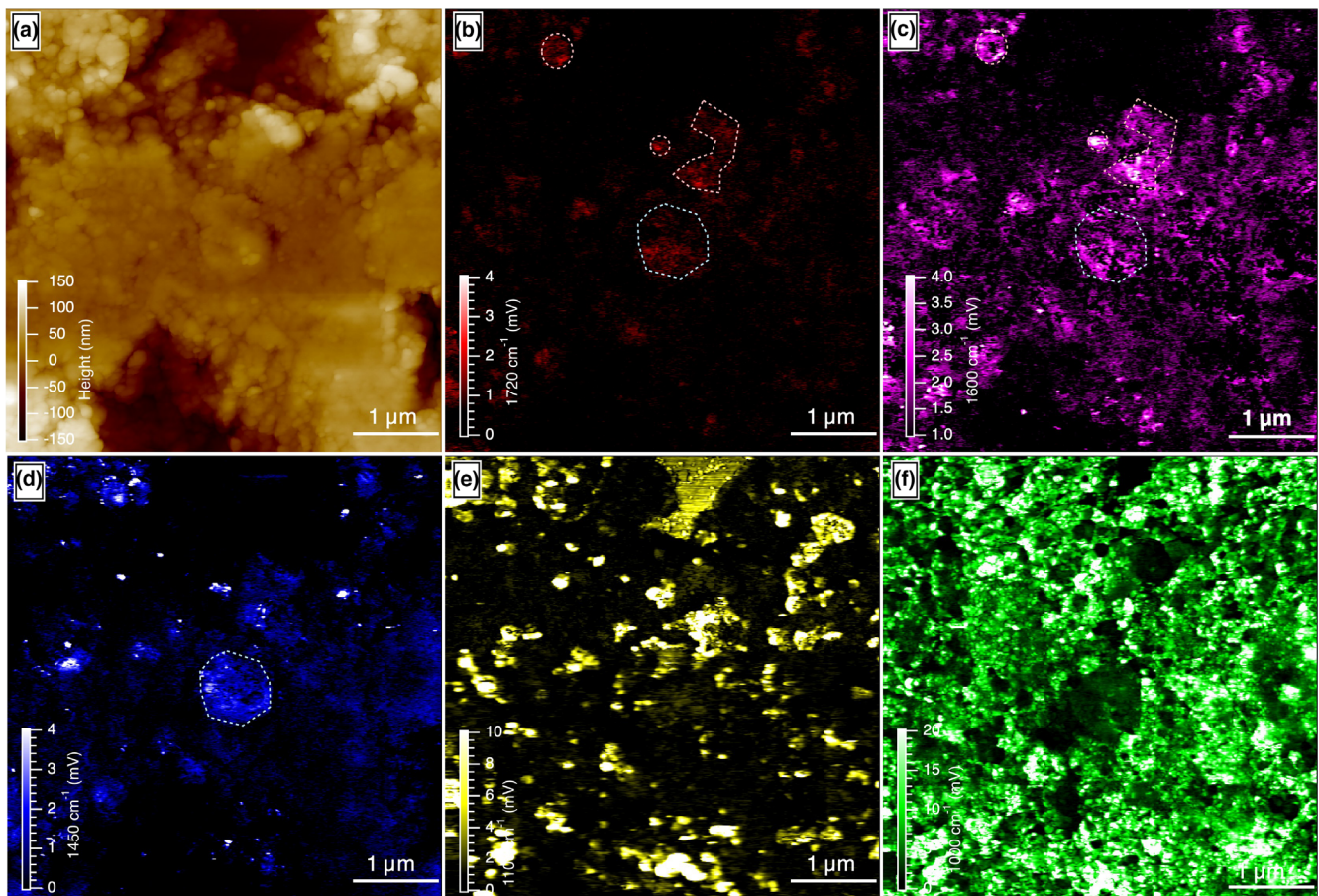


FIGURE 1. C0105-0032. (a) Topographic image (AFM) of the region of interest (ROI of $5 \times 5 \mu\text{m}^2$); Chemical images of the absorption band at (b) C O at 1720 cm^{-1} , (c) C C and/or water at 1600 cm^{-1} , (d) carbonate and/or CH_2 bending mode at 1450 cm^{-1} , (e) SO_4 and/or wing of Si-O at 1100 cm^{-1} , and (f) Si-O at 1000 cm^{-1} .

A $20 \times 20 \mu\text{m}^2$ area of grain 3 (G3) (red spectra in Figure 3) was imaged in AFM-IR tapping mode (Figure 4). Different from C0105-0032 grain, this grain does not display a signature around 1100 cm^{-1} , meaning that sulfate is absent. Similarly, AFM-IR intensity was measured at 1720 , 1450 , and 1000 cm^{-1} , corresponding to carbonyl (C O), carbonate (CO_3), and phyllosilicate (Si-O) (Figure 4c–e). These maps and the associated RGB composite map we produced (Figure 4f) show an intense signal at 1000 cm^{-1} throughout the sample (green) that can be attributed to phyllosilicate. This map also shows grains with strong AFM-IR intensity in all three wavelengths (bright green in the RGB composite) that are interpreted to be phases with high refractive index (Fe-oxides, metal, and sulfides) which was confirmed by SEM imaging and is corroborated by other studies (Dartois et al., 2023). Several small grains appear in blue in this map and are interpreted to be small carbonate grains.

Interestingly, a small circular area in the right bottom corner of the map shows a strong signature at 1720 cm^{-1} (Figure 4c,f) corresponding to C O in organic matter. An

array of 50 spectra was collected in the green zone (Si-O array) and one spectrum (A1) was obtained on the “red globule” in the RGB composite map (Figure 4b,f). In addition to the organic globule, organic signatures are present as a diffuse component within the phyllosilicate (average Si-O spectra), as evidenced from the presence of aromatic (C C) band at 1600 cm^{-1} (Figure 4g) and a small feature around 1720 cm^{-1} . In the average spectra of “green” areas, a broad band around 1000 cm^{-1} is present, similar to results obtained from grain C0105-0032, and attributed to Si-O in phyllosilicates. Note that in the phyllosilicate-rich areas, the water bending mode at 1630 cm^{-1} can contribute to some extent to this spectral region. While Ryugu grains analyzed following an air-shutoff procedure do not show strong evidence for molecular water (Nakamura et al., 2022), our samples that were exposed to air probably experienced rehydration to some extent.

The A1 spectrum obtained on the red globule shows three distinct peaks at 1720 , 1600 , and 1450 cm^{-1} attributed to the C O, C C, and CH_2 bending mode in

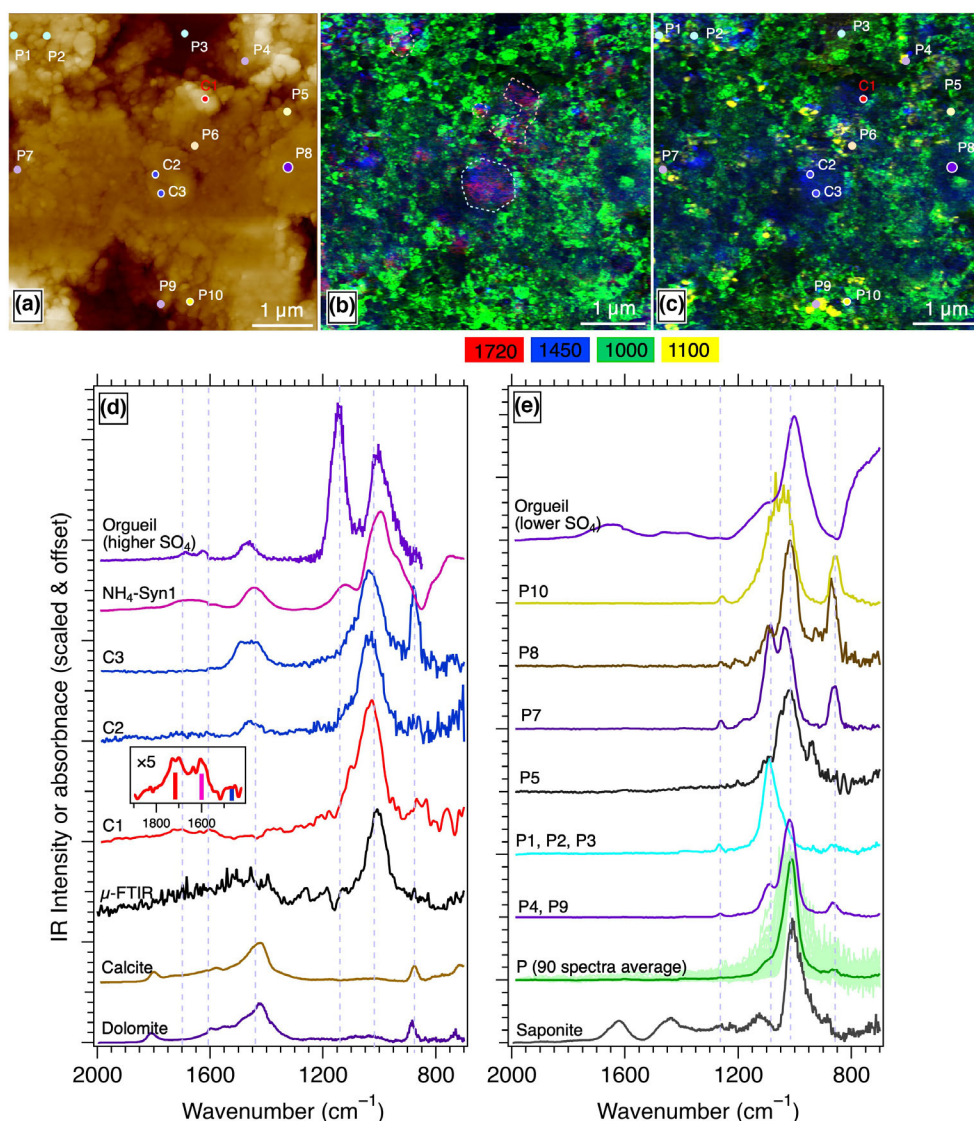


FIGURE 2. C0105-0032. (a) Topographic image (AFM) with the single-point AFM-IR spectral positions surrounding the $5 \times 5 \mu\text{m}^2$ image (labeled C1: red point, C2, C3: blue point, P1–P10); (b) A composite image at 1720, 1000, and 1450 cm^{-1} ; (c) a composite image at 1450, 1000, and 1100 cm^{-1} ; (d) comparison between the single-point AFM-IR spectra in carbonate-rich regions and the average μ -FTIR spectrum of same Ryugu grain, AFM-IR spectra of carbonate references (dolomite, calcite) and $\text{NH}_4\text{-Syn-1}$ (*Ammonium-mica-montmorillonite*); the AFM-IR spectra of Orgueil with high sulfate; (e) comparison between AFM-IR spectra of phyllosilicate-rich regions, AFM-IR spectra of saponite and Orgueil with lower sulfate.

organic matter (Figure 4g). This spectrum is reminiscent of infrared spectra obtained on insoluble organic matter (Orthous-Daunay et al., 2013; Quirico et al., [this volume](#)), or organic particle found in Orgueil (Phan et al., 2022) (Figure 4g).

Comparison to μ -FTIR spectra obtained on the same grain reveals a good consistency between local AFM-IR and conventional μ -FTIR spectra (Figure 4g). The μ -FTIR spectra (in black) can be well explained by a mixture of average AFM-IR phyllosilicate spectra and carbonates (to explain the 1450 cm^{-1} slightly more

elevated in the FTIR spectrum of the grain than in the average AFM-IR spectrum of phyllosilicates) and the different probe depths of the two techniques.

While no phyllosilicate signal was detected in the globule area, the AFM-IR spectra reveal a broad absorption massif with a maximum around 1050 cm^{-1} . The fact that no signal was detected in the AFM-IR map is related to the fact that AFM-IR maps are obtained in tapping mode, more sensitive to the surface, while AFM-IR spectra are obtained in contact mode, that probes a larger volume of sample. The different shape of the

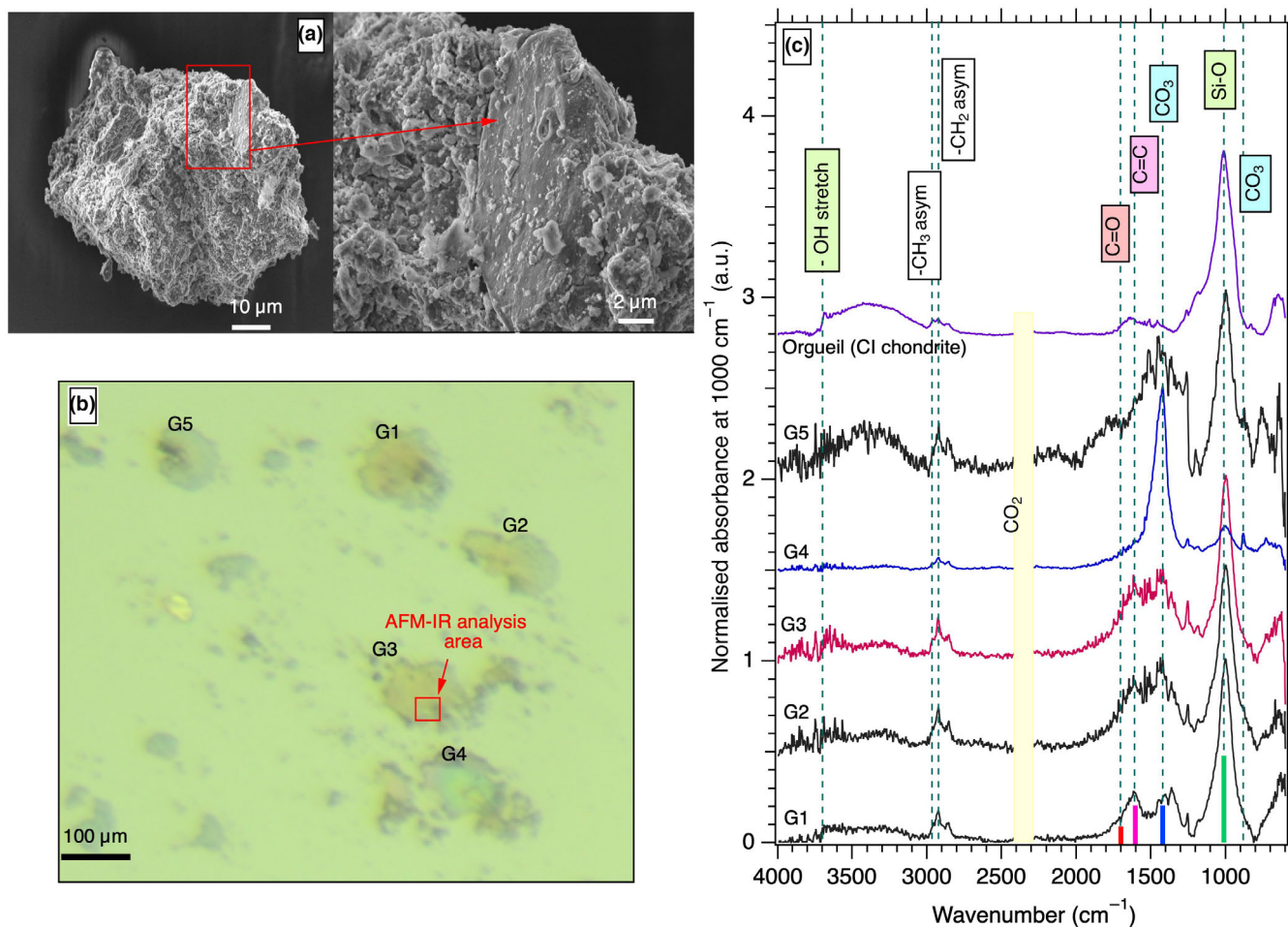


FIGURE 3. C0105-0038. μ -FTIR spectra of Ryugu sample in different grains. (a) Backscattered electron (BSE) image showing the melted splash due to the space weathering (Noguchi et al., 2023). (b) Visible image of different fractured grains after crushing between two diamond windows (G1–G5) for μ -FTIR analysis, the red square shows the location of the AFM-IR map. (c) Different μ -FTIR spectra corresponding to G1–G5 grains in the visible image (b) in comparison to μ -FTIR spectrum of Orgueil (CI chondrite).

$1000\text{--}1050\text{ cm}^{-1}$ band between the organic globule and typical Ryugu phyllosilicate is related to the presence of a different type of silicate (amorphous?) or contribution from organic vibration to this spectral region.

To further elucidate the mineralogy and structure of the organic matter in this area, we collected AFM-IR maps of a $3 \times 3\ \mu\text{m}^2$ area (Figure 5a) around the organic globule at wavelengths similar to those used for the larger area (1720 , 1600 , 1450 , and 1000 cm^{-1}) shown in Figure 5b–e). As can be seen in Figure 5f, this region shows a significant contribution from the Si-O stretching of the phyllosilicates in the 1000 cm^{-1} map, but these contributions are absent in the central organic-rich area. Conversely, the central part corresponding to the organic globule shows a strong 1720 cm^{-1} absorption related to C O. The region also exhibits infrared absorptions at 1600 and 1450 cm^{-1} as shown in Figure 5c,d, which are

spatially correlated and can be attributed to aromatic (C C) or/and water molecules, and aliphatic organic compounds, respectively. In addition, the IR maps also show areas with strong and correlated intensity at 1600 , 1450 , and 1000 cm^{-1} , which may reveal the presence of high refractive index Fe-bearing minerals such as Fe sulfide and Fe-Ni sulfides (Dartois et al., 2023), as shown in the Fe, Ni, S, and BSE EDS images obtained after the AFM-IR measurement (Figures S1 and S2).

The micro-globule apparent in the 1720 cm^{-1} absorption image is circular and has a diameter of $\sim 1\ \mu\text{m}$ (Figure 5f). This globule was further investigated with full AFM-IR spectra (Figure 6) at the locations indicated in the AFM composite images (Figure 6a,b). The first spectrum at the central globule location (A1) reveals two distinct peaks and shows a higher aromatic peak intensity (C C) at 1600 cm^{-1} and less carbonyl (C O) at 1720 cm^{-1}

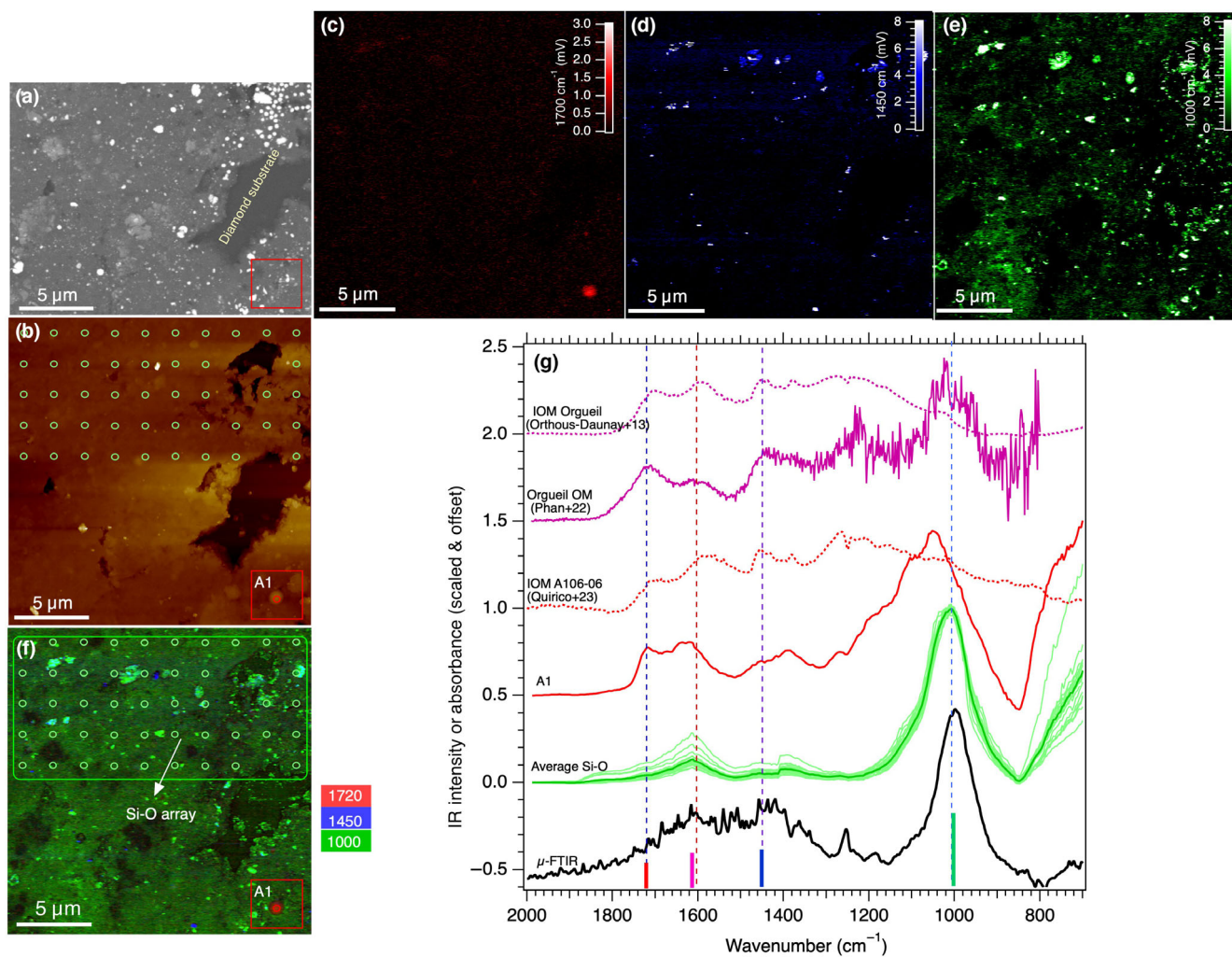


FIGURE 4. C0105-0038 ($20 \times 20 \mu\text{m}^2$). (a) SEM image showing the region of AFM-IR measurements using the APE laser in the $2000\text{--}700 \text{ cm}^{-1}$ range. (b) Topographical image of the $20 \times 20 \mu\text{m}^2$ area. AFM-IR images collected at different absorption band at (c) C O at 1720 cm^{-1} (in red); (d) carbonate and/or CH_2 bend mode at 1450 cm^{-1} (in blue); (e) Si-O at 1000 cm^{-1} (in green); and (f) composite RGB image in tapping mode of the three maps: 1720 , 1000 , and 1450 cm^{-1} , respectively, with a small organic globule is visible in red square surrounded by a dominant phyllosilicate in green; (g) comparison between AFM-IR single point spectra in the locations shown in (b) and (f), the μ -FTIR spectrum of Ryugu G3 grain, IOM Ryugu A106-06 (Quirico et al., [this volume](#)), IOM Orgueil (Orthous-Daunay et al., 2013), and the AFM-IR spectra of organic particles in Orgueil (Phan et al., 2022).

than in the bulk organic particles we analyzed in Orgueil (Figure 6c) (Phan et al., 2022). The weak peak at 1450 cm^{-1} is attributed to the CH_2 bending mode, carbonate or NH_4^+ bending mode, which are all in this spectral area. Although the sample IR images show no signal at 1000 cm^{-1} (Figure 5e), the contact IR spectrum reveals a prominent peak at 1050 cm^{-1} that has moved from the phyllosilicate position at 1000 cm^{-1} (Figures 4g and 6c,d), following results obtained in our first investigations of the globule.

A series of spectra were collected in the globule from the center outward (labeled A1–A8 and B1–B8) in positions shown in the AFM and RGB images

(Figure 6a,b) to better understand the variation of the organic and silicate structure inside and outside the organic globule. The spectra obtained are consistent with the presence of macromolecular organics as part of the globule. As can be seen, the CH_2 and CH_3 bending modes (1450 and 1380 cm^{-1}) or the broad congested band $\sim 1250 \text{ cm}^{-1}$ (C O, C C, OH, etc.) appear in all spectra within the globule (e.g., A1–A6 and B1–B4) and are consistent with observation of IOM in chondrites using conventional μ -FTIR spectroscopy (Kebukawa et al., 2011; Orthous-Daunay et al., 2013). In these spectra, we also confirm the presence of the broad absorption massif with a maximum around 1050 cm^{-1} .

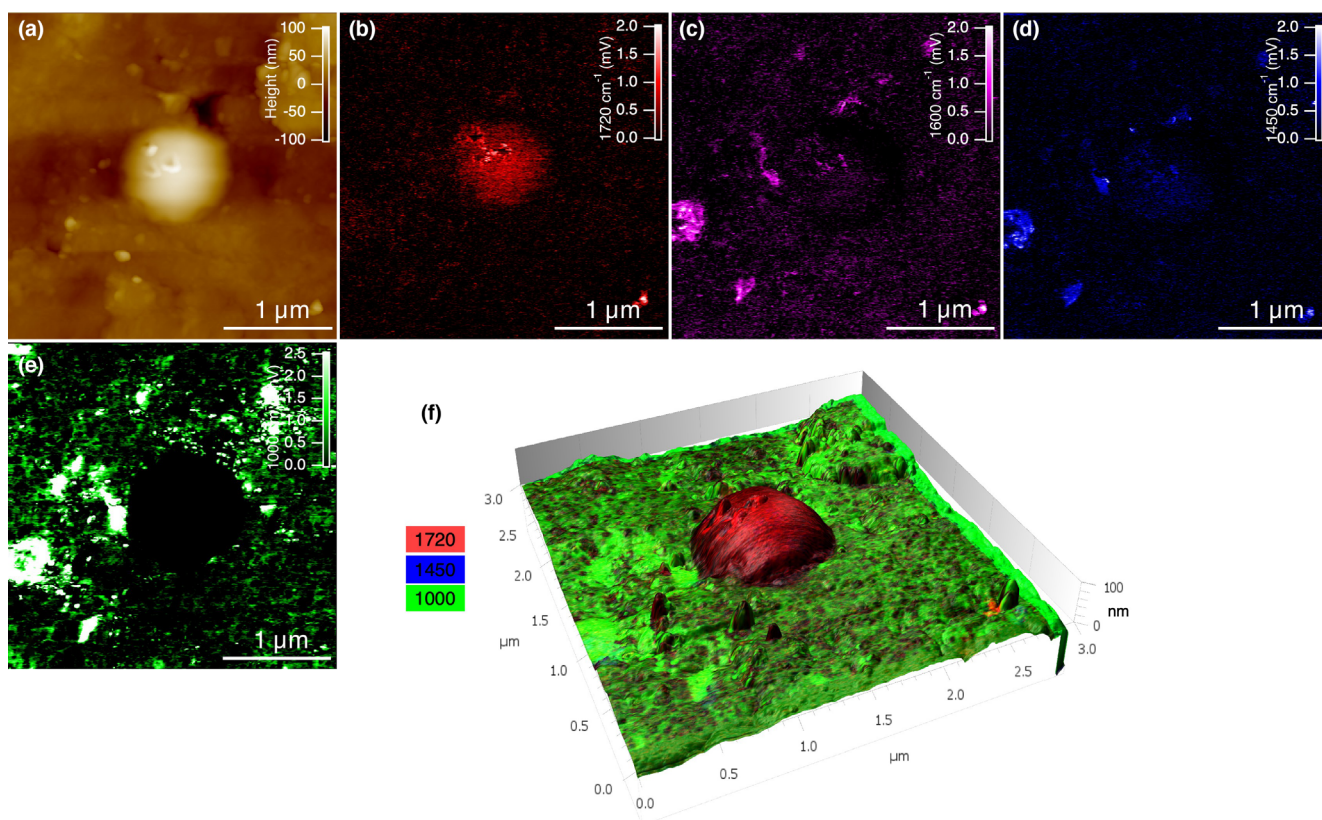


FIGURE 5. C0105-0038 ($3 \times 3 \mu\text{m}^2$). (a) Topographical image (AFM) showing some small spots damaged due to the physical contact of the AFM tip; absorption images of the bands (b) C O at 1720 cm^{-1} ; (c) C C and water at 1600 cm^{-1} ; (d) $\text{CO}_3^-/\text{CH}_2$ bending mode at 1450 cm^{-1} ; (e) Si-O at 1000 cm^{-1} ; (f) composite 3-D view of the RGB image derived from the three maps: 1720, 1000, and 1450 cm^{-1} , respectively, showing the “lentil” shape of the globule.

Looking at the relative intensity of the C O and C C modes, the organic structure appears to be increasingly less aromatic while the silicate peak shape becomes thinner from the center outward (Figure 6c,d).

DISCUSSION

Infrared Mineralogy and Comparison with Other Extraterrestrial Materials

The silicate mineralogy of Ryugu fine-grained samples is dominated by a mixture of “coarse”- and “fine”-grained phyllosilicates, with chemical compositions intermediate between saponite and serpentine (Noguchi et al., [this volume](#)). The presence of saponite and serpentine domains was confirmed by high-resolution bright-field TEM (Noguchi et al., [this volume](#)). Serpentine and saponite are expected to have different mid-infrared spectra in the $10 \mu\text{m}$ range where Si-O stretching occurs, at least in the case of well-crystallized serpentines (Beck et al., 2014; Dartois et al., 2023). Interestingly, the serpentine-rich CM chondrites like ALH 83100 have infrared spectra in the

$10 \mu\text{m}$ range clearly distinct from CI-chondrites (Figure 7), meaning that even low-crystallinity serpentines, generally dominate the mineralogical composition in CM chondrites, can be distinguished from saponite; accordingly, a band is more in line with serpentine measurement. Based on IR, the mineralogy of our Ryugu “sands” seems related to saponite, rather than serpentine or a mixture of both.

Ryugu samples from the IOM and stone team were investigated with similar techniques by Dartois et al. (2023). In their work, the spectral range covered is similar to that in our study (slightly broader in Dartois et al. (2023) as it goes down to 100 cm^{-1}). A difference between these two works is that, in our case, FTIR measurements were done in a custom-made environmental cell enabling exposure of the sample to vacuum and gentle heating (80°C). This procedure enables to remove weakly bonded water molecules. Overall, the FTIR spectra we obtained on fine-grained samples from the sand team are highly similar to those obtained by Dartois et al. (2023), and the AFM-IR images and spectra obtained in both works are in agreement. Therefore, the combination of our work and Dartois et al. (2023) reveals a certain

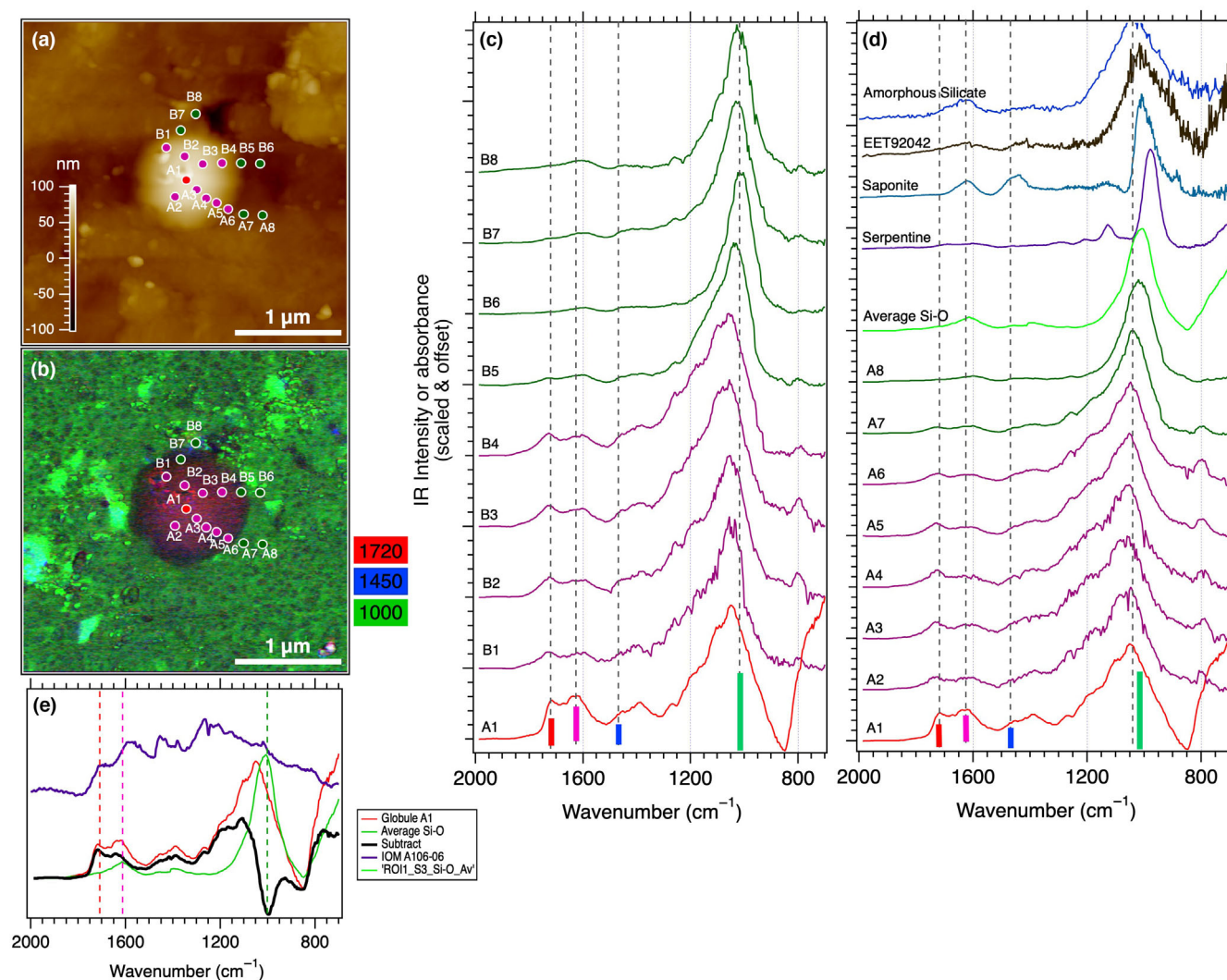


FIGURE 6. C0105-0038-G3. (a) AFM and (b) composite 2-D view of the RGB image derived from three AFM-IR images at 1720, 1450, and 1000 cm^{-1} , respectively, with the location of the single point AFM-IR spectra; (c) AFM-IR spectra performed in selected positions indicated in (a) and (b) images (labeled b1–b8); (d) the AFM-IR spectra performed in selected positions shown in (a) and (b) images (labeled a1–a8) from the center to exterior of the organic globule, in comparison with mixture of saponite and carbonate, serpentine and amorphous silicate (anhydrous silicate) (Potapov et al., 2020), and AFM-IR spectrum of amorphous silicate in carbonaceous chondrite EET 92042 (Phan et al., 2022); (e) The subtracted spectrum between the organic globule (A1 spectrum) and the average Si-O spectrum, in comparison with μ -FTIR spectrum of IOM A106-06 (Quirico et al., this volume).

homogeneity of Ryugu mineralogy over a range of grain sizes.

Spectra of CI chondrites show a shoulder around 1200 cm^{-1} that can be related to the presence of sulfates, and this shoulder is absent from Ryugu samples. At least a fraction of sulfates minerals in CI chondrites are interpreted to be of terrestrial origin (Gounelle & Zolensky, 2001, 2014; Nakamura et al., 2022; Viennet et al., 2023) and samples from Ryugu are fresher in that sense. Still, we observed that one of the samples studied shows signature of small sulfate grains (<1 μm) than can

be interpreted as products from the fast terrestrial oxidation of iron sulfides. The signatures of carbonates at 880 and 1450 cm^{-1} present in the spectra of the ungrouped carbonaceous chondrites Tarda and Tagish Lake (Figure 7) are absent in the spectra of the Ryugu grain shown in Figure 7, but carbonates were identified with AFM-IR and in other grains with μ -FTIR analyses.

Overall, from an infrared point of view, the clay mineralogy of Ryugu is similar to other CI chondrites, some lithologies of Tagish Lake, and some other samples belonging to the magnetite- and ^{17}O -rich group of

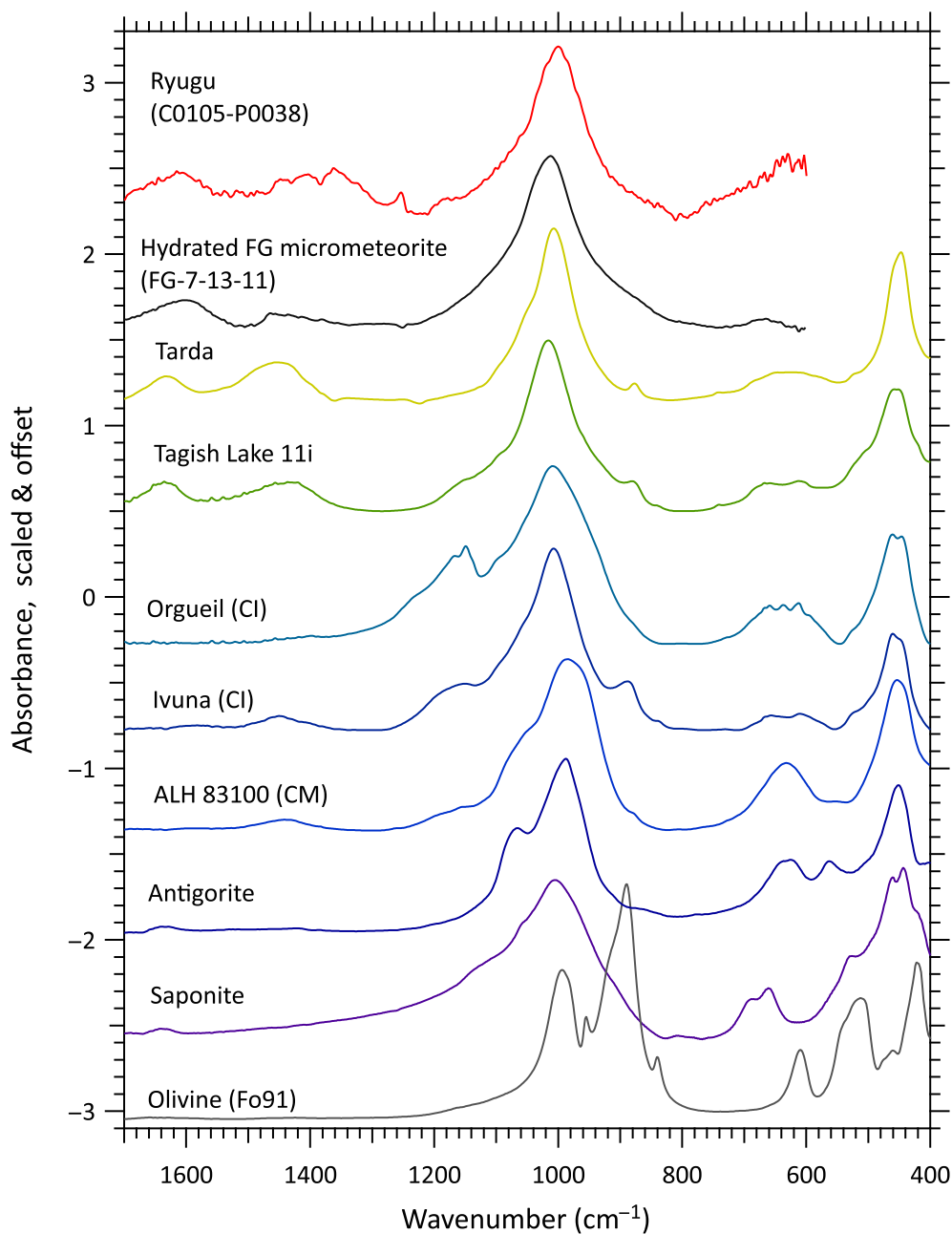


FIGURE 7. Comparison of the MIR spectra of Ryugu grain C0105-0038 to CI chondrites (Orgueil and Ivuna from Beck et al., 2014), ungrouped carbonaceous chondrites (Tarda and Tagish Lake from Gilmour et al., 2019), a CM chondrite, and reference mineral phases (Beck et al., 2014).

carbonaceous chondrites (Figure 7, Hewins et al., 2021). It is interesting to note that these meteorites, in addition to having some commonalities from a chemical point of view, also present some similarities in the clay mineralogy. We also present in Figure 7, a typical spectrum obtained on a fine-grained hydrated micrometeorite from Battandier et al. (2018). We can observe in this graph that hydrated micrometeorites are similar to Ryugu samples and CI chondrites, and clearly distinct from CM chondrites

(Figure 7). The similarities between Ryugu, CI chondrites, hydrated IDPs, and micrometeorites are also discussed in Noguchi et al. (this volume).

An Organic Micro-Globule

While organic globules had been observed in different types of meteorites (e.g., Alexander et al., 2017; Claus & Nagy, 1961), the discovery of an organic globule

analyzed in situ (without liquid or acid extraction) and on a fresh meteorite fall (Tagish Lake) provided clear and nonambiguous evidence for an extraterrestrial origin of at least some of the globules (Nakamura et al., 2002). While these structures are often referred to as “nano”-globules, their size range goes up to more than a micrometer in diameter (140–1700 nm in Nakamura et al., 2002; 150–1150 nm in De Gregorio et al., 2013). We will refer here to the term globule to describe a spherical organic grain (>100 nm), that may contain a mineral grain in its interior (and in that case it is equivalent to a spherical coating). The globules can be solid or hollow, and may present some layering in their interior (Vollmer, Pelka, et al., 2020). They are made of H-, O-, and N-bearing organic carbon and can be host to isotopic enrichment for C, N, or H, but not systematically and variably (De Gregorio et al., 2013; Nakamura-Messenger et al., 2006; Vollmer, Leitner, et al., 2020). For example, some nanoglobules from ALH 77307, Murchison, and Orgueil were not isotopically enriched (De Gregorio et al., 2013). They were also found to have different organo-chemistry, with some globules enriched in aromatic moieties, while others having a composition more similar to insoluble organic matter (IOM) (De Gregorio et al., 2013). In the case of Ryugu sample, a carbon nanoglobule was observed by Ito et al. (2022), which was hosting a silicate phase in its interior. Hollow and solid nanoglobules have also been observed in IOM samples extracted from Ryugu grains, and showing both aromatic-rich and IOM compositions (Yabuta et al., 2023).

Physical Properties of this “Lentil” Globule

The AFM-IR probe configuration in our measurements is not able to distinguish whether the globule we observed is solid or hollow (Figure 5f). We note, however, that based on the combined 3-D view of AFM topography and RGB composite maps, the globule is not flat or spherical but “lentil” shaped (Figure 5f). The AFM topographical image shows its apparent diameter is around 1 μm , while the physical height of the shape protruding from Ryugu phyllosilicates matrix is only around 100 nm. This “lentil” shape could be related to sample preparation, but we would rather expect a flat surface in that case. This shape may represent the original structure of the globule, but most of it is buried in the surrounding matrix. An alternative possibility is that the globule was hollow, with a spherical shape and collapsed at some point.

After our investigations on the globule in the 7–13 μm range with the APE laser source, we attempted to characterize its aliphatic linkage using the Firefly laser source (2.5–4 μm). For hardware reason, chemical

mapping using this laser source was only possible using AFM contact mode, and not tapping mode like for the APE source. This mapping led to the disruption of the globule and the organics that were constituting the globule were somehow spread over the surface (see SI, Figures S3 and S4). We also note that the areas for which APE spectra were collected (in contact mode) are visible in the AFM-IR map obtained after spectral measurements (Figure 5b). The three small pits are due to the indentation of the globule by the AFM-tip. This attests that the globule is somehow weak in physical nature.

The Nature of Organic Matter in Fine-Grained Samples and in the Globule

Organic compounds were investigated by several techniques in Ryugu samples and revealed a direct link between macromolecular organic matter in C-type asteroids and that in primitive carbonaceous chondrites. Four main chemical forms of carbon have been observed in Ryugu grains as diffuse, highly aromatic, aromatic, and IOM-like organic matter. Particles and globules tend to show more highly carbonyl and aromatic compositions, while diffuse organics more dispersed throughout the sample resemble IOM-like organic matter (Yabuta et al., 2023). In the present study, both organic globule and diffuse organics in fine-grained Ryugu were observed by AFM-IR measurements. The spectral range covered by the APE laser can in principle be used to obtain information on the aromaticity of the organic compounds, provided that the contribution of carbonates to the 1450 cm^{-1} feature (CH_2 group) is negligible. In that case, the ratio of the 1450 and 1650 cm^{-1} (aromatic C C) band can be used as a semiquantitative tracer of aromaticity. Nevertheless, molecular water in the phyllosilicate may lead to a spectral superposition between the organic C C and C O bands and the water bending mode around 1630 cm^{-1} , which can be removed by heating the sample in vacuum with conventional $\mu\text{-FTIR}$ (Beck et al., 2010; Orthous-Daunay et al., 2013) but cannot be removed with our AFM-IR setup.

In the case of two C0105 grains, diffuse organics seem to be present based on the AFM-IR maps but the spectral range where the doublet of bands at 1720 and 1600 cm^{-1} occurs (attributed to C O and C C) is perturbed by the water bending mode. The intensity ratio of C O and C C is significantly lower than that of Ryugu IOM from $\mu\text{-FTIR}$ spectra (Quirico et al., [this volume](#)) (Figure 8), suggesting a contribution of water to the C C position near 1600 cm^{-1} or that diffuse organics are less carbonylated than IOM. Peak fitting by Dartois et al. (2023) to disentangle between molecular water and

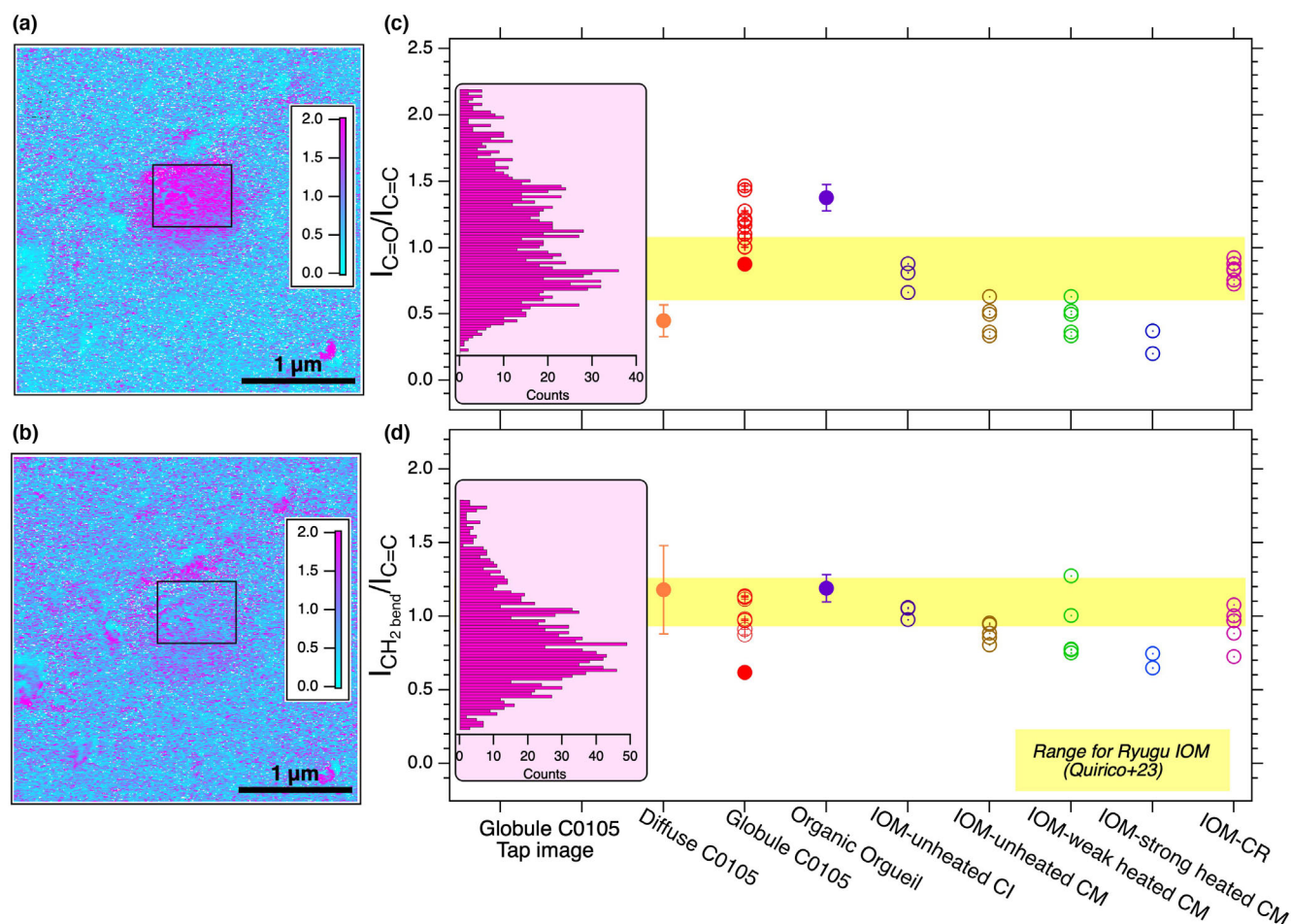


FIGURE 8. C0105-0038. The AFM-IR ratio images showing (a) the I_{1720}/I_{1600} and (b) I_{1450}/I_{1600} ratio of interest region ($3 \times 3 \mu\text{m}^2$) for C0105-0038. Comparison of the peak intensity ratio of (c) C O and C C bands at 1720 and 1600 cm^{-1} , respectively, and (d) CH_2 bending mode and C C bands at 1450 and 1600 cm^{-1} , respectively, including: Histogram of the I_{1720}/I_{1600} ratio extracted from (a), histogram of the I_{1450}/I_{1600} extracted from (b), the contact AFM-IR spectra of the organic globule in “bulk” Ryugu in C0105-0038, the AFM-IR spectra of the organic particle in Orgueil (Phan et al., 2022), the μ -FTIR spectra of IOM-like Ryugu from Quirico et al. (this volume) in yellow bar, and the μ -FTIR spectra of various IOMs in carbonaceous chondrites (Quirico et al., 2018).

C C signatures seems to show that at least some grains have a contribution from aromatic-rich organics in this spectral range.

Aliphatic organics are present in Ryugu fine-grained samples as evidenced by the modes around $3.4\text{--}3.4 \mu\text{m}$ seen in our conventional μ -FTIR spectra, which cannot be due to globules given their rarity, and which has been observed through STEM-EELS-EDS (Yabuta et al., 2023). This diffuse aliphatic organic fraction is similar to that of Orgueil (Le Guillou & Brearley, 2014; Phan et al., 2022). It has been suggested that some of these compounds may be hosted within the interlayer space of phyllosilicates (Viennet et al., 2023). The comparison between spectra of intact Ryugu grains and IOM shows that the CH_2/CH_3 ratio determined from the ratio of the antisymmetric stretching modes of the CH_2 and CH_3

chemical groups is higher for intact grains compared to IOM (Dartois et al., 2023; Quirico et al., this volume) (Figure S4). This supports the view that diffuse organic matter is a mix between IOM and soluble organic molecules that are lost during the chemical extraction of IOM.

The AFM-IR spectra obtained on the globule are presented in Figure 6, while some structural parameters ($\text{C O}/\text{C C}$ and $\text{CH}_2\text{bend}/\text{C C}$) derived from these spectra are shown in Figure 8a,b. At first glance, the spectra obtained on the globule are reminiscent of measurements obtained on IOM samples (Quirico et al., this volume). A difference is the presence of a broad absorption at 1050 cm^{-1} that we attribute to silicates under or inside the globule (see discussion below). Some spectral variations were found inside the globule, with an increase

of the C O/C C and CH₂bend/C C from the center to the exterior (Figure 8) of the globule. Overall, these parameters are in line with values obtained for Ryugu's IOM (Figure 8), revealing that the organic chemistry of the globule is similar to IOM.

The IOM PET team analyzed in detail the organo-chemistry of refractory organics from Ryugu samples, as well as their isotopic composition (Yabuta et al., 2023). Organic globules were found and investigated by several techniques revealing the presence of both IOM-like and aromatic globules, with grain size ranging typically 50–500 nm up to 2000 nm in diameter. The globule we investigated here is therefore among the largest ones found in Ryugu so far. Both IOM-like and aromatic globules were found in Yabuta et al. (2023), while the only globule we detected is IOM-like. However, aromatic globules may be more difficult to detect with AFM-IR due to the interference with molecular water, and the lack of 1720 cm⁻¹ peak.

Silicates Inside the Globule?

The organic globule identified by Ito et al. (2022) in Ryugu samples revealed the presence of a silicate particle in its interior. A carbon globule with a silicate core was also observed in the CR2 chondrite NWA 801 (Hashiguchi et al., 2013) and in Renazzo-type CR chondrites GRA 95229 (Vollmer, Pelka, et al., 2020). In our case, while the AFM-IR maps obtained in tapping mode revealed the absence of signal in the Si-O region in the globule, contact mode spectra showed the presence of a broad band around 1050 cm⁻¹, probably due to silicate signature for AFM-IR spectra obtained within the globule. Contact mode AFM-IR spectra may probe a larger volume around several micrometers under the surface (Mathurin, Deniset-Besseau, et al., 2022) and may be picking signals from below or inside the globule. Given the diameter of the globule and the spatial resolution of contact mode IR spectra (Phan et al., 2022), it is unlikely that this silicate signature comes from the phyllosilicates on the side of the globule. It can also be noted that this silicate signature is distinct from typical phyllosilicates signatures obtained from Ryugu samples, with a broader shape and maxima of absorption around 1050 cm⁻¹. The spectra obtained on the globule also show a feature around 800 cm⁻¹, not seen in other spectra obtained on Ryugu. This band could be related to Si-O-Si bending in SiO₂ or to Fe³⁺-OH in a phyllosilicate (Madejová et al., 2017). The fact that this silicate signature is particular and was found only associated with the globule may suggest that this phase may be located inside the globule. However, this argument remains circumstantial at best without excavation and direct observation of the grain interior.

Possible Formation Mechanisms

We typically surveyed an area of more than 2500 μm² fine-grained Ryugu samples with AFM-IR, while the surface of the nanoglobule is <1 μm². Therefore, carbon-rich globules are rare and the amount of C present in the form of globules is likely insufficient to be the dominant reservoir of carbon in Ryugu samples since the bulk organic C content is about 3 wt% (Yokoyama et al., 2022). Several possible formation mechanisms and formation environments have been proposed for the carbon-rich globules encountered in carbonaceous chondrites. They were summarized in the thorough investigation by De Gregorio et al. (2013). The possible formation environments include presolar, solar nebula, or asteroidal. If they are presolar, these globules may be inherited directly from the diffuse interstellar medium (DISM) with the observation of the high abundance of aromatic groups (Dartois et al., 2007), where carbonaceous compounds could form a shell surrounding an ice and silicate core (Greenberg et al., 1995). In the solar nebula scenario, carbon globules may be the leftovers of gas-phase or solid-state chemistry in the solar parent molecular cloud or the protosolar nebula. Globular-shape carbon-rich particles have been produced experimentally by two-step UV irradiation of ice mixture (Piani et al., 2017) or warm plasma chemistry (Bekaert et al., 2018). However, the capability of such a mechanism to reproduce the peculiar structure of IOM remains to be assessed (Quirico et al., 2020). A last formation environment that has been proposed for carbon-rich globules is on the parent planetesimal, where their formation would be triggered by the presence of liquid water on these objects. In the study of Cody et al. (2011), micrometer-sized globule with morphologies reminiscent of meteorite observations were produced from the liquid-phase polymerization of formaldehyde. Another possibility is that the presence of liquid water on the asteroid could have induced the mobilization of a diffuse organic fraction and led to their condensation locally. In that sense, the organic globule would form as coatings surrounding a pre-existing grain such as discussed by Vollmer, Pelka, et al. (2020).

In our study, only one globule was observed, but for the first time, we were able to extract the IR spectra of a single globule, in situ. Our observation reveals strong similarities with insoluble organic matter, and that this globule is not particularly enriched in aromatic moieties. This IOM-like chemistry is consistent with analyses on IOM extracted from the CI Orgueil by De Gregorio et al. (2013), for which no aromatic globule was found unlike CR chondrites for instance. In our work, we observed some chemical variability within the globule based on the C O/C C ratio, where the outer part of the globule appears enriched in C O. This may record

the history of the globule synthesis, or its chemical modification upon hydrothermal alteration.

The fact that the globule seems to be associated with a silicate phase distinct from the typical phyllosilicates from Ryugu, as observed in Ito et al. (2022) and our study, suggests that the globule was not produced on the asteroid; in the parent body mechanisms suggested in the above paragraph, none would lead to preferential formation of the globule around a specific type of silicates. One possibility is that the migration and coalescence of organic compounds occurred at the very beginning of the aqueous alteration process, and the presence of the coating protected the silicate from conversion to phyllosilicates. While parent body formation cannot be strictly excluded, our preferred explanation is a pre-accretionary origin, but the exact environment and synthesis mechanism remain elusive. The oxygen isotope of the silicates associated with the carbon globule in the CR2 chondrite NWA 801 was measured by Hashiguchi et al. (2013). Their results showed that oxygen isotopes in the silicate are similar to solar system material, suggesting then a solar system origin for the globule. Similar work done on Hayabusa2 samples may help understand the formation environment of the carbon globules from Ryugu.

CONCLUSION

Here, we report on an infrared spectroscopy study of fine-grained particles from the Ryugu asteroid, as part of the Hayabusa2 PET “sand” team. Infrared absorption properties were obtained on grains at the $100 \times 100 \mu\text{m}$ scale using conventional FTIR and at the sub- μm scale using photothermal AFM-IR.

This work confirms that the mineralogy of Ryugu fine-grained material is dominated by phyllosilicates. These phyllosilicates are Mg-rich and have infrared properties similar to saponite, based on the $10 \mu\text{m}$ silicate absorption feature. They are clearly distinct from CM chondrites, and similar to observations on other CI chondrites or selected ungrouped carbonaceous chondrites, as well as to some hydrated micrometeorites. The sulfate signature seen in CI chondrites is absent from our FTIR spectra of Ryugu samples. We also observe carbonate ion signatures in the transmission FTIR spectra, and these ions are expected to be present in a dolomite crystallographic structure.

Further investigations of the Ryugu “sands” mineralogy and organic compounds were performed using AFM-IR, enabling to probe the sub- μm scale. We observe little variability of the Si-O stretching, showing a relative homogeneity of the phyllosilicate from an IR perspective at that scale. We observe the presence of small carbonate grains (100–500 nm) finely mixed with the phyllosilicate. In one of the studied areas, small

particles associated with a band at 1100 cm^{-1} are present and interpreted to be terrestrial sulfate forming at the expense of S-bearing opaques.

Analysis of organic signatures reveals the presence of a diffuse organic component, from the presence of CH modes, and we observe a single carbon-rich globule from AFM-IR mapping. This globule is roughly $1 \mu\text{m}$ in diameter and AFM-IR spectra obtained revealed the presence of CO and CC, and CH₂-bend, in a similar way to IOM extracted from Ryugu samples. From our study, carbon globule is rare in Ryugu and likely represents only a fraction of the carbon budget in Ryugu; however, detection biases may be present and inherent to our technique and sample preparation protocol. This globule seems to be associated with silicate whose nature is different from the typical Ryugu phyllosilicate. The presence of IOM like globules in Orgueil was observed by De Gregorio et al. (2013) after acid leaching. Our in situ AFM-IR analysis reveals the existence of such globule in a CI-related object. A pre-accretion scenario is favored for the formation of this globule, but the exact formation environment and mechanisms remain elusive.

Acknowledgments—The Hayabusa2 project has been developed and led by JAXA in collaboration with Deutsches Zentrum für Luft- und Raumfahrt (DLR) and Centre national d'études spatiales (CNES), and supported by NASA and Australian Space Agency (ASA). We thank all of the members of the Hayabusa2 project for their technical and scientific contributions. This research was supported by the H2020 European Research Council (ERC) (SOLARYS ERC-CoG2017_771691) and the Programme National de Planétologie (PNP) as well as the Centre national d'études spatiales (CNES) within the framework of the Hayabusa 2 and MMX missions. We also acknowledge Frédéric Charlot for the assistance during SEM/EDS analysis at CMTC (Grenoble, France). All of the sources of funding for the work described in this publication are acknowledged below: The Hayabusa2 project has been developed and led by JAXA in collaboration with Deutsches Zentrum für Luft- und Raumfahrt (DLR) and Centre national d'études spatiales (CNES), and supported by NASA and Australian Space Agency (ASA). The H2020 European Research Council (ERC) (SOLARYS ERC-CoG2017_771691). The Programme National de Planétologie (PNP). The Centre national d'études spatiales (CNES) within the framework of the Hayabusa 2 and MMX missions.

Conflict of Interest Statement—We wish to confirm that there are no known conflicts of interest associated with this publication and there has been no significant financial support for this work that could have influenced its outcome.

Data Availability Statement—The data that support the findings of this study are available from the corresponding author upon reasonable request.

Editorial Handling—Dr. Edward Anthony Cloutis

REFERENCES

- Alexander, C. M. O'D., Cody, G. D., De Gregorio, B. T., Nittler, L. R., and Stroud, R. M. 2017. The Nature, Origin and Modification of Insoluble Organic Matter in Chondrites, the Major Source of Earth's C and N. *Chemie Der Erde* 77: 227–256. <https://doi.org/10.1016/j.chemer.2017.01.007>.
- Battandier, M., Bonal, L., Quirico, E., Beck, P., Engrand, C., Duprat, J., and Dartois, E. 2018. Characterization of the Organic Matter and Hydration State of Antarctic Micrometeorites: A Reservoir Distinct from Carbonaceous Chondrites. *Icarus* 306: 74–93. <https://doi.org/10.1016/j.icarus.2018.02.002>.
- Beck, P., Garenne, A., Quirico, E., Bonal, L., Montes-hernandez, G., Moynier, F., and Schmitt, B. 2014. Transmission Infrared Spectra (2–25 μm) of Carbonaceous Chondrites (CI, CM, CV–CK, CR, C2 Ungrouped): Mineralogy, Water, and Asteroidal Processes. *Icarus* 229: 263–277. <https://doi.org/10.1016/j.icarus.2013.10.019>.
- Beck, P., Quirico, E., Montes-Hernandez, G., Bonal, L., Bollard, J., Orthous-Daunay, F. R., Howard, K. T., et al. 2010. Hydrous Mineralogy of CM and CI Chondrites from Infrared Spectroscopy and their Relationship with Low Albedo Asteroids. *Geochimica et Cosmochimica Acta* 74: 4881–92. <https://doi.org/10.1016/j.gca.2010.05.020>.
- Bekaert, D. V., Derenne, S., Tissandier, L., Marrocchi, Y., Charnoz, S., Anquetil, C., and Marty, B. 2018. High-Temperature Ionization-Induced Synthesis of Biologically Relevant Molecules in the Protosolar Nebula. *The Astrophysical Journal* 859: 142. <https://doi.org/10.3847/1538-4357/aabe7a>.
- Claus, G., and Nagy, B. 1961. A Microbiological Examination of some Carbonaceous Chondrites. *Nature* 192: 594–96. <https://doi.org/10.1038/192594a0>.
- Cody, G. D., Heying, E., Alexander, C. M. O'D., Nittler, L. R., Kilcoyne, A. L. D., Sandford, S. A., and Stroud, R. M. 2011. Establishing a Molecular Relationship between Chondritic and Cometary Organic Solids. *Proceedings of the National Academy of Sciences of the United States of America* 108: 19171–76. <https://doi.org/10.1073/pnas.1015913108>.
- Dartois, E., Geballe, T. R., Pino, T., Cao, A.-T., Jones, A., Deboffe, D., Guerrini, V., Bréchnignac, P., and D'Hendecourt, L. 2007. IRAS 08572+3915: Constraining the Aromatic Versus Aliphatic Content of Interstellar HACs. *Astronomy & Astrophysics* 463: 635–640. <https://doi.org/10.1051/0004-6361>.
- Dartois, E., Kebukawa, Y., Yabuta, H., Mathurin, J., Engrand, C., Duprat, J., Bejach, L., et al. 2023. Chemical Composition of Carbonaceous Asteroid Ryugu from Synchrotron Spectroscopy in the Mid- to Far-Infrared of. *Astronomy & Astrophysics* 671: 1–30.
- Dazzi, A., and Prater, C. B. 2017. AFM-IR: Technology and Applications in Nanoscale Infrared Spectroscopy and Chemical Imaging. *Chemical Review* 117: 5146–73. <https://doi.org/10.1021/acs.chemrev.6b00448>.
- De Gregorio, B. T., Stroud, R. M., Nittler, L. R., Alexander, C. M. O'D., Bassim, N. D., Cody, G. D., Kilcoyne, A. L. D., et al. 2013. Isotopic and Chemical Variation of Organic Nanoglobules in Primitive Meteorites. *Meteoritics & Planetary Science* 48: 904–928. <https://doi.org/10.1111/maps.12109>.
- Gilmour, C. M., Herd, C. D., and Beck, P. 2019. Water Abundance in the Tagish Lake Meteorite from TGA and IR Spectroscopy: Evaluation of Aqueous Alteration. *Meteoritics & Planetary Science* 54: 1951–72.
- Gounelle, M., and Zolensky, M. E. 2001. A Terrestrial Origin for Sulfate Veins in CI Chondrites. *Meteoritics & Planetary Science* 36: 1321–29. <https://doi.org/10.1111/j.1945-5100.2001.tb01827.x>.
- Gounelle, M., and Zolensky, M. E. 2014. The Orgueil Meteorite: 150 Years of History. *Meteoritics & Planetary Science* 49: 1769–94. <https://doi.org/10.1111/maps.12351>.
- Greenberg, J. M., Li, A., Mendoza-Gómez, C. X., Schutte, W. A., Gerakines, P. A., and de Groot, M. 1995. Approaching the Interstellar Grain Organic Refractory Component. *The Astrophysical Journal* 455: 177–180. <https://doi.org/10.1086/309834>.
- Hashiguchi, M., Kobayashi, S., and Yurimoto, H. 2013. In Situ Observation of D-Rich Carbonaceous Globules Embedded in NWA 801 CR2 Chondrite. *Geochimica et Cosmochimica Acta* 122: 306–323. <https://doi.org/10.1016/j.gca.2013.08.007>.
- Hewins, R. H., Zanetta, P. M., Zanda, B., Le Guillou, C., Gattacceca, J., Sognzoni, C., Pont, S., et al. 2021. NORTHWEST AFRICA (NWA) 12563 and Ungrouped C2 Chondrites: Alteration Styles and Relationships to Asteroids. *Geochimica et Cosmochimica Acta* 311: 238–273. <https://doi.org/10.1016/j.gca.2021.06.035>.
- Ito, M., Tomioka, N., Uesugi, M., Yamaguchi, A., Shirai, N., Ohigashi, T., Liu, M.-C., et al. 2022. A Pristine Record of Outer Solar System Materials from Asteroid Ryugu's Returned Sample. *Nature Astronomy* 6: 1163–71. <https://doi.org/10.1038/s41550-022-01745-5>.
- Jubb, A. M., Hackley, P. C., Hatcherian, J. J., Qu, J., and Nesheim, T. O. 2019. Nanoscale Molecular Fractionation of Organic Matter within Unconventional Petroleum Source Beds. *Energy Fuel* 33(10): 9759–66. <https://doi.org/10.1021/acs.energyfuels.9b02518>.
- Kebukawa, Y., Alexander, C. M. O'D., and Cody, G. D. 2011. Compositional Diversity in Insoluble Organic Matter in Type 1, 2 and 3 Chondrites as Detected by Infrared Spectroscopy. *Geochimica et Cosmochimica Acta* 75: 3530–41. <https://doi.org/10.1016/j.gca.2011.03.037>.
- Kebukawa, Y., Kobayashi, H., Urayama, N., Baden, N., and Kondo, M. 2018. Nanoscale Infrared Imaging Analysis of Carbonaceous Chondrites to Understand Organic-Mineral Interactions during Aqueous Alteration. *Proceedings of the National Academy of Sciences of the United States of America* 1–6: 753–58. <https://doi.org/10.1073/pnas.1816265116>.
- Le Guillou, C., Bernard, S., Brearley, A. J., and Remusat, L. 2014. Evolution of Organic Matter in Orgueil, Murchison and Renazzo during Parent Body Aqueous Alteration: In Situ Investigations. *Geochimica et Cosmochimica Acta* 131: 368–392. <https://doi.org/10.1016/j.gca.2013.11.020>.
- Le Guillou, C., and Brearley, A. 2014. Relationships between Organics, Water and Early Stages of Aqueous Alteration in the Pristine CR3.0 Chondrite MET 00426. *Geochimica et Cosmochimica Acta* 131: 344–367. <https://doi.org/10.1016/j.gca.2013.10.024>.
- Madejová, J., Gates, W. P., and Petit, S. 2017. IR Spectra of Clay Minerals. *Developments in Clay Science* 8: 107–149. <https://doi.org/10.1016/B978-0-08-100355-8.00005-9>.

- Mathurin, J., Dartois, E., Pino, T., Engrand, C., Duprat, J., Deniset-besseau, A., Borondics, F., Sandt, C., and Dazzi, A. 2019. Nanometre-Scale Infrared Chemical Imaging of Organic Matter in Ultra-Carbonaceous Antarctic Micrometeorites (UCAMMs). *Astronomy & Astrophysics* 160: 1–9.
- Mathurin, J., Deniset-Besseau, A., Bazin, D., Dartois, E., Wagner, M., and Dazzi, A. 2022. Photothermal AFM-IR Spectroscopy and Imaging: Status, Challenges, and Trends. *Journal of Applied Physics* 131: 010901. <https://doi.org/10.1063/5.0063902>.
- Nakamura, K., Zolensky, M. E., Tomita, S., Nakashima, S., and Tomeoka, K. 2002. Hollow Organic Globules in the Tagish Lake Meteorite as Possible Products of Primitive Organic Reaction. *International Journal of Astrobiology* 1: 179–189.
- Nakamura, T., Matsumoto, M., Amano, K., Enokido, Y., Zolensky, M. E., Mikouchi, T., Genda, H., et al. 2022. Formation and Evolution of Carbonaceous Asteroid Ryugu: Direct Evidence from Returned Samples. *Science* 379: eabn8671.
- Nakamura-Messenger, K., Messenger, S., Keller, L. P., Clemett, S. J., and Zolensky, M. E. 2006. Organic Globules in the Tagish Lake Meteorite: Remnants of the Protosolar Disk. *Science* 314: 1439–42.
- Naraoka, H., Takano, Y., Dworkin, J. P., Oba, Y., Hamase, K., Furusho, A., Ogawa, N. O., et al. 2023. Soluble Organic Molecules in Samples of the Carbonaceous Asteroid (162173) Ryugu. *Science* 379(6634): 162173. <https://doi.org/10.1126/science.abn9033>.
- Noguchi, T., Matsumoto, R., Yabuta, H., Kobayashi, H., Miyake, A., Naraoka, H., Okazaki, R., et al. 2022. Antarctic Micrometeorite Composed of CP and CS IDP-Like Material: A Micro-Breccia Originated from a Partially Ice-Melted Comet-like Small Body. *Meteoritics & Planetary Science* 57: 2042–62. <https://doi.org/10.1111/maps.13919>.
- Noguchi, T., Matsumoto, T., Miyake, A., Igami, Y., Haruta, M., Saito, H., Hata, S., et al. 2023. A Dehydrated Space Weathered Skin Cloaking the Hydrated Interior of Ryugu. *Nature Astronomy* 7: 170–181.
- Noguchi, T., Matsumoto, T., Miyake, A., Igami, Y., Haruta, M., Saito, H., Hata, S., et al. this volume. Mineralogy and Petrology of Fine-Grained Samples Recovered from the Asteroid (162173) Ryugu. *Meteoritics & Planetary Science*.
- Orthous-Daunay, F. R., Quirico, E., Beck, P., Brissaud, O., Dartois, E., Pino, T., and Schmitt, B. 2013. Mid-Infrared Study of the Molecular Structure Variability of Insoluble Organic Matter from Primitive Chondrites. *Icarus* 223: 534–543. <https://doi.org/10.1016/j.icarus.2013.01.003>.
- Phan, V. T. H., Quirico, E., Beck, P., Le Brech, Y., Jovanovic, L., Le Guillou, C., Bernard, S., et al. 2021. Infrared Spectroscopy Quantification of Functional Carbon Groups in Kerogens and Coals: A Calibration Procedure. *Spectrochimica Acta—Part A: Molecular and Biomolecular Spectroscopy* 259: 119853. <https://doi.org/10.1016/j.saa.2021.119853>.
- Phan, V. T. H., Rebois, R., Beck, P., Quirico, E., Bonal, L., and Noguchi, T. 2022. Nanoscale Mineralogy and Organic Structure in Orgueil (CI) and EET 92042 (CR) Carbonaceous Chondrites Studied with AFM-IR Spectroscopy. *Meteoritics & Planetary Science* 57: 3–21. <https://doi.org/10.1111/maps.13773>.
- Phan, V. T. H., Rebois, R., Beck, P., Quirico, E., Noguchi, T., and Takase, M. 2023. Chemical Functional Characterization of Immature and Mature Coals at the Nanoscale by Atomic Force Microscopy-Based Infrared Spectroscopy (AFM-IR). *International Journal of Coal Geology* 267: 104196. <https://doi.org/10.2139/ssrn.4253550>.
- Piani, L., Tachibana, S., Hama, T., Tanaka, H., Endo, Y., Sugawara, I., Dessimoulie, L., et al. 2017. Evolution of Morphological and Physical Properties of Laboratory Interstellar Organic Residues with Ultraviolet Irradiation. *The Astrophysical Journal* 837: 35. <https://doi.org/10.3847/1538-4357/aa5ca6>.
- Potapov, A., Bouwman, J., Jäger, C., and Henning, T. 2020. Dust/Ice Mixing in Cold Regions and Solid-State Water in the Diffuse Interstellar Medium. *Nature Astronomy* 5: 78–85. <https://doi.org/10.1038/s41550-020-01214-x>.
- Quirico, E., Bonal, L., Kebukawa, Y., Amano, K., Yabuta, H., Phan, V. T. H., Beck, P., et al. this volume. Compositional Heterogeneity of Insoluble Organic Matter Extracted from Hayabusa 2 Samples. *Meteoritics & Planetary Science*.
- Quirico, E., Bonal, L., Beck, P., Alexander, C. M. O'D., Yabuta, H., Nakamura, T., Nakato, A., et al. 2018. Prevalence and Nature of Heating Processes in CM and C2-Ungrouped Chondrites as Revealed by Insoluble Organic Matter. *Geochimica et Cosmochimica Acta* 241: 17–37. <https://doi.org/10.1016/j.gca.2018.08.029>.
- Quirico, E., Bonal, L., Montagnac, G., Beck, P., and Reynard, B. 2020. New Insights into the Structure and Formation of Coals, Terrestrial and Extraterrestrial Kerogens from Resonant UV Raman Spectroscopy. *Geochimica et Cosmochimica Acta* 282: 156–176. <https://doi.org/10.1016/j.gca.2020.05.028>.
- Tomeoka, K., and Buseck, P. R. 1988. Matrix Mineralogy of the Orgueil CI Carbonaceous Chondrite. *Geochimica et Cosmochimica Acta* 52: 1627–40. [https://doi.org/10.1016/0016-7037\(88\)90231-1](https://doi.org/10.1016/0016-7037(88)90231-1).
- Viennet, J.-C., Roskosz, M., Nakamura, T., Beck, P., Baptiste, B., Lavina, B., Alp, E. E., et al. 2023. Interaction between Clay Minerals and Organics in Asteroid Ryugu. *Geochemical Perspectives Letters* 25: 8–12. <https://doi.org/10.7185/geochemlet.2307>.
- Vollmer, C., Leitner, J., Kepaptsoglou, D., Ramasse, Q. M., King, A. J., Schofield, P. F., Bischoff, A., Araki, T., and Hoppe, P. 2020. A Primordial ¹⁵N-Depleted Organic Component Detected within the Carbonaceous Chondrite Maribo. *Scientific Reports* 10: 1–9. <https://doi.org/10.1038/s41598-020-77190-z>.
- Vollmer, C., Pelka, M., Leitner, J., and Janssen, A. 2020. Amorphous Silicates as a Record of Solar Nenular and Parent Body Processes—A Transmission Electron Microscope Study of Fine-Grained Rims and Matrix in Three Antarctic CR Chondrites. *Meteoritics & Planetary Science* 55: 1491–1508.
- Yabuta, H., Cody, G. D., Engrand, C., Kebukawa, Y., De Gregorio, B., Bonal, L., Remusat, L., et al. (2023). Macromolecular Organic Matter in Samples of the Asteroid (162173) Ryugu. *Science* 379: eabn9057.
- Yada, T., Abe, M., Okada, T., Nakato, A., Yogata, K., Miyazaki, A., Hatakeda, K., et al. 2021. Preliminary Analysis of the Hayabusa2 Samples Returned from C-type Asteroid Ryugu. *Nature Astronomy* 6: 214–220. <https://doi.org/10.1038/s41550-021-01550-6>.
- Yesiltas, M., Glotch, T. D., and Kaya, M. 2021. Nanoscale Infrared Characterization of Dark Clasts and Fine-Grained Rims in CM2 Chondrites: Aguas Zarcas and Jbilet Winselwan. *Earth and Space Chemistry* 5: 3281–96. <https://doi.org/10.1021/acsearthspacechem.1c00290>.

Yokoyama, T., Nagashima, K., Nakai, I., Young, E. D., Abe, Y., Aléon, J., Alexander, C. M. O'D., et al. 2022. Samples Returned from the Asteroid Ryugu are Similar to Ivuna-

type Carbonaceous Chondrites. *Science* 379. <https://doi.org/10.1126/science.abn7850>.

SUPPORTING INFORMATION

Additional supporting information may be found in the online version of this article.

FIGURE S1. (a, b) BSE images of C0105-0032 and C0105-0038 of AFM-IR measurement area. (c) EDS spectra of C0105-0032 with spot locations shown in (a). (d) EDS spectra of C0105-0038 with spot locations shown in (b).

FIGURE S2. C0105-0038-G3. (a) Backscattered electron (BSE) image displaying the region interest (ROI) with AFM-IR analysis. (b) EDS composition map of nickel (Ni in cyan) and sulfur (S in orange). (c) EDS map of silicon (Si in green) and (d) EDS composition map of sulfur (S in orange) and silicon (Si in green).

FIGURE S3. C0105-0038-G3. AFM-IR maps recorded using the Firefly (FF) laser in the 3800–2700 cm^{-1} range. (a) Topographical image. (b) OH stretching at 3680 cm^{-1} (green); (c) CH_3 asymmetric

(blue); and (d) CH_2 asymmetric (red) at 2960 and 2930 cm^{-1} , respectively. (e) RG (red, green) composite image of the two maps: 3680 and 2930 cm^{-1} , respectively, and (f) RGB (red, green, blue) composite image of the three maps: 3680, 2930, and 2960 cm^{-1} , respectively.

FIGURE S4. C0105-0038-G3. AFM-IR maps recorded using the Firefly (FF) laser in the 4000–2700 cm^{-1} range. (a) Topographical image with the spectral locations. (b) RGB (red, green, blue) composite image of the three maps at 2930, 3680, and 2960 cm^{-1} , respectively. (c) Average AFM-IR spectra collected in the green area located in (a, b) with the presence of OH stretch at 3680 cm^{-1} and aliphatic organic in the range of 3000–2800 cm^{-1} . (d) Average AFM-IR spectra collected in the organic globule located in (a, b) with less signal of OH stretching at 3680 cm^{-1} and aliphatic organic in the range of 3000–2800 cm^{-1} , in comparison with μ -FTIR spectrum of IOM Ryugu A106-06 (Quirico et al., submitted).